Thesis for the Degree of Master

A Compact Circularly Polarized MIMO Dielectric Resonator Antenna Over Electromagnetic Bandgap Surface for 5G Applications

Advisor: Professor Jung-Dong Park

Graduate School of Dongguk University

Department of Electrical and Electronic Engineering

Hsiang Nerng Chen

2020

Thesis for the Degree of Master

A Compact Circularly Polarized MIMO Dielectric Resonator Antenna Over Electromagnetic Bandgap Surface for 5G Applications

by

Hsiang Nerng Chen

Advisor: Professor Jung-Dong Park

Date of submission : 2019/12

Date of approval : 2020/01

Approved by:

Chairman : Professor Hyun-Chang Park (Sign)

Committee member : Professor Han-Ho Choi (Sign)

Committee member : Professor Jung-Dong Park (Sign)

Graduate School of Dongguk University

ACKNOWLEDGEMENTS

I would like to express my sincere gratitude to my advisor Prof. Jung-Dong Park for his thoughtful guidance, constructive feedback and advises throughout my master's degree. His support and encouragement have allowed me to receive the SRD-II scholarship and successfully made a publication in a SCIE journal as a lead author.

Special thanks to my lab mates Van-Son Trinh, Van-Viet Nguyen, Young Joe Choi, Jeong Moon Song and senior Hyohyun Nam for their assistance during my research.

Lastly, I would like to thank my parents for their undying support throughout my entire tenure in Korea.

ABSTRACT

본 논문에서는 다이버시티가 강화된 광 대역 원형편파(CP) 특성을 가지는 다중입력 다중출력(MIMO) 유전체 공진기 안테나(DRA)를 제시한다. 광 대역 원형 편파 DRA 를 구현하기 위해 DRA 의 두 대각선 모서리를 45°로 잘라서 5G 대역폭 내에서 0.65GHz 보다 큰 축 비(AR)를 구현했다. DRA 는 FR4 기판 하단에 구현된 마이크로 스트립 라인 에서 특정 슬롯/ 암 비율을 가진 십자 링 슬롯에 의해 확장된 CP 필드를 생성 한다. 또한 DR 의 가장자리에 있는 작은 삼각 기둥 형 스탠드를 사용하여 DR 을 기판에 부착하는 데 사용되는 접착제로 인한 변인을 차단 하였다. DRA 는 4.83dBi 의 이득과 함께 0.8GHz 보다 넓은 임피던스 대역폭을 달성했다. 마이크로 스트립 라인 구조를 사용하여 두 개의 CP DRA 배열을 구현하고, 기판 상면에 식각된 EBG 구조를 사용했다. 제안된 구조는 작은 크기를 유지하면서 성능 저하 없이 원하는 주파수 대역에서 26dB 보다 더 높은 격리성(isolation)을 달성했다. 구현된 원형 편파 MIMO DRA 에 대하여 다이버시티 분석이 수행되었다. 측정 결과는 시뮬레이션과 잘 일치 하였으며, 이는 제안된 기법이 소형 크기의 광 대역 원형 편파 MIMO 안테나 시스템을 구현하기에 적합함을 입증했다.

ABSTRACT

In this thesis, a wideband circularly polarized (CP) multiple-input multiple-output (MIMO) dielectric resonator antenna (DRA) with enhanced diversity is presented. To implement a wideband circularly polarized DRA element, two diagonal edges of the DRA were truncated at 45° to obtain a wider axial ratio (AR) larger than 0.65 GHz for 5G bandwidth. The DRA element was excited by a cross-ring slot with specific slot-arm ratio through microstrip line implemented at the bottom side of the FR4 substrate to generate CP fields. Furthermore, small triangular stands at the edge of the DR were employed to hold it in place which avoided unwanted effects from the uncontrollable bonding agent used to attach the DR onto the substrate. The DRA achieved an impedance bandwidth wider than 0.8 GHz with a gain of 4.83 dBi. By using the DRA element with the microstrip line feed, two element CP DRA array was implemented with electromagnetic bandgap (EBG) structure etched onto the ground plane. The proposed structure achieved isolation better than 26 dB over the desired frequency band without any performance degradation while maintaining its compact size in the array. Diversity analysis were performed on the implemented circularly polarized MIMO DRA. The measured results corresponded quite well with simulations, which demonstrated that the proposed technique is suitable for implementing wideband circular polarized MIMO antenna systems with compact size.

ABBREVIATIONS

AR	Axial Ratio
CP	Circular Polarization
LP	Linear Polarization
LHCP	Left-hand Circular Polarization
RHCP	Right-hand Circular Polarization
HFSS	High Frequency Structure Simulator
EM	Electromagnetic
FEM	Finite Element Method
EBG	Electromagnetic Bandgap
MIMO	Multiple-Input Multiple-Output
PBC	Periodic Boundary Conditions
PML	Perfectly Matched Layer
ECC	Envelope Correlation Coefficient
CCL	Channel Capacity Loss

Table of Contents

LIST OF FIGURES

LIST OF TABLES

Chapter 1 INTRODUCTION

1.1 Introduction to Dielectric Resonator Antennas

In 1939, Richtmyer initially demonstrated microwave resonators in the form of non-metallized dielectric objects in theory [1]. Due to the properties of these structures, it was then named as dielectric resonators (DR). The modes of these dielectric entities were later analyzed by Okaya and Barash in the early 1960s [2], which then gradually led to historic developments in various circuit applications including filters, oscillators and amplifiers towards the late 1960s. However, these dielectric resonators possess high-Q (low-loss) characteristics and are usually shielded to prevent radiation. Richtmyer also mentioned that a DR would be capable to radiate if placed in a free space caused by boundary conditions at the interface of dielectric and air.

The concept of dielectric resonators as antenna elements, also known as dielectric resonator antenna (DRA) was first proposed by S.A. Long in 1983 [3]. In his transaction, a cylindrical DR providing efficient radiation in the direction normal to its ground plane is demonstrated. Since then, in-depth research has been taken place on the analysis of DRA material properties and its effectiveness. Numerous shapes, resonant modes, radiation characteristics and excitation techniques of the DRA have been proposed along with reputable journal publications by Junker et. al. [4], Lee and Simons [5], Leung et. al. [6], Luk et. al. [7], Mongia et. al. [8], Petosa et. al. [9] and many others till date. The outcome of these investigations which sums the attractive features of most DRAs are as follows:

- Comprehensible design concept. The DRA dimensions are in proportion to free-space wavelength, λ_0 at designated resonant frequency and ε_r is the material's dielectric constant;
- Design flexibility. For a fixed dielectric constant, resonant frequency and radiation Q-factor of DRAs can be controlled by the aspect ratio.
- Wide range of dielectric constants. From the range of 8 to 100, the physical size and bandwidth of the DRA can be controlled accordingly.
- Wide range of operational frequencies. Published state-of-the-art designs have been recorded from 1.3 GHz to 40 GHz.

- Various excitation methods. Examples are coaxial probe, aperture-coupling with microstrip feedline, aperture coupling with coaxial feedline, direct microstrip feedline, co-planar feed, slotline, stripline, conformal strip etc. [10].

In summary, high degree of flexibility and versatility of the DRA allows antenna designers to deal with a wide range of physical and electrical requirements of different communication applications today.

1.2 Circularly Polarized Dielectric Resonator Antenna

Circular polarization (CP) can be produced if the sum of electric fields has two orthogonal components having the same magnitude and 90° phase difference between the two components. The polarization state of an EM wave is most commonly indicated by Axial Ratio (AR). AR is a key parameter often used to characterize the degree of circular polarization, whereby AR of a CP antenna is generally required to be below 3 dB [11].

For decades, research on DRAs have been concentrated on linear polarization (LP). However, circularly polarized dielectric resonator antennas (CPDRAs) are generally preferred due to their insensitivity towards antenna misalignment and propagation effects [12]. In contrast, an LP signal is not capable of being properly received when the transmitter is orthogonal to the field. Reported multi-feed structures have shown wide axial ratio (AR) bandwidth of a CPDRA with additional external power divider or quadrature coupler, thus increasing the system size and complexity [13], [14].

As compact wideband systems are in high demand for recent wireless communication, numerous techniques for single point fed designs have been explored up until now. Various shapes of CP-DRAs aimed with wide AR bandwidth have been published, such as stair-shape [15], DR with outer-fed square spiral strip [16], hollow DR [17], slotted DR with parasitic strips [18], and DR with inclined slits [19], [20]. Slot excitation methods on DR having dual-resonance and broadband features, was first introduced by Buerkle et al. [21] has been applied often due to fabrication simplicity, low cross-polarization levels and nonnegligible back radiation advantages. The method has then been further utilized in [22], [23] and [24] which

consists of dual-band and broadband circularly polarized operations, aiming at GPS & WLAN applications. Other recent slot design techniques for CP involved are the logarithmic spiral slot [25] and plus-shaped slot [26]. However, investigations on truncation or partial truncated DRA with slot patterns catering wide CP characteristics in the S-band frequency range is still uncommon.

1.3 MIMO Circularly Polarized DRA

Most recently, multiple-input multiple-output (MIMO) technologies has been in continuous development for wireless communication systems. It is also known that MIMO antenna systems are widely used for wireless local networks (WLAN), long-term evolution (LTE), and ultimately fifth generation (5G) communication soon.

The requirement for compact MIMO antennas arises to accommodate mobile terminals and base stations for less space consumption and aesthetic reasons [27]. One of the critical considerations in implementing MIMO antenna system is by exhibiting low mutual coupling between radiating elements. MIMO antennas utilizing microstrip patch designs often have lower efficiencies and weak isolation between unit antennas, which causes it to be unsuitable in frequently used applications [28]. To counter such issue, compact DRAs with high radiation efficiency will be much preferable, no undesirable effects in array configurations with improved isolation can be observed.

Numerous literatures on reducing mutual coupling between DRA elements has been proposed. Defected ground plane structures (DGS) attracts attention by altering the surface waves, which then reduces mutual coupling. A fractal DRA with defected ground structures (DGS) performs with an enhanced isolation up to 15 dB [29]. In a similar manner, Maltese-shaped DRAs on C-shaped periodic DGS shows significant reduction in mutual coupling [30]. On the other hand, several electromagnetic bandgap (EBG) structures have been implemented in DRAs as well. A design utilizing EBG structure achieved a 13 dB isolation [31]. Metasurface shield through the side split-ring resonators (SRR) configuration exhibit reduction in mutual coupling, however, at a much higher frequency band and with the trade-off of degradation in radiation pattern [32]. In another relevant research, a metamaterial polarization-rotator wall (MPR) placed between cylindrical DRAs have been

proposed with a 16 dB reduction in mutual coupling [33]. Nevertheless, the above-mentioned literatures are generally linearly polarized and responsive to performance degradation due to misalignment issues [34]. As of today, there is little to no significant research performed on circularly polarized MIMO DRAs, except for a few recorded literatures to counter misalignment difficulties and concentrates on multi-band applications [34]-[37]. An effective mutual coupling reduction hybrid structure has been proposed in [38] for a wideband circular polarized MIMO DRA. However, the diagonally placed DR elements increases the overall antenna size approximately $4.3\lambda_0$, which can be practically inconvenient for many applications.

1.4 Motivation of this Work

Nowadays, high quality ubiquitous wireless communication system is required more than ever before. Ever since 4G technology has been deployed, researchers are eyeing towards future 5G communication technology. This new 5G technology arose from the need for an improvement in internet, performance and cost [39]. NGMN (Next Generation Mobile Networks) has a vision that in year 2020, the 5G technology will develop a realm which establishes an entirely mobile and linked society. 5G is expected to support several use cases with a great diversity of applications such as broadband access in dense areas. Communications will be able to take place in multistory structures, dense urban city centers and events in the presence of thousands of people [40].

In the beginning of April 2019, Samsung Electronics has celebrated its first delivery of 5G technology to South Korea. All three major Korean mobile service provider such as KT, SK Telecom and LG Uplus are currently offering 5G services commercially available for consumers and enterprises in more than 80 cities. All 3 main Korean operators are utilizing Samsung's 5G Massive-MIMO Unit (MMU) radio base station at 3.5 GHz [41].

In this thesis, a compact wideband circularly polarized DRA for 5G applications (3.3–3.8 GHz) in the Republic of Korea is proposed. Through optimization of the design parameters, resonances of the dielectric-loaded cross-ring slot antenna and cross-ring slot excited DRA can be combined to attain a wide AR performance and an improved impedance bandwidth. Furthermore, effects of common adhesives on

the AR and input impedance of the DRA was examined, whereby deterioration in AR performance is observed. To avoid undesirable use of adhesive, two small DR posts are introduced at the diagonal corners to lock it in position without interfering its radiation characteristics. Lastly, a MIMO array configuration of the proposed CPDRA utlizing EBG structure is proposed as well. Whereby low envelope correlation coefficient (ECC), high diversity gain (DG) and low channel capacity loss (CCL) is achieved while maintaining its overall compact size.

Chapter 2 ANTENNA CONFIGURATION

2.1 Rectangular Dielectric Resonator Antenna Design

The resonant frequency of a rectangular dielectric resonator antenna is usually determined through the well-known dielectric waveguide model (DWM) [42], [43]. However, Fang & Leung [44] have further simplified the engineering formula without the use of advance programming. Fundamental TE^{y}_{111} mode and higher-order TE^{y}_{113} mode can be utilized to design a dual-mode antenna. By setting two arbitrary resonance frequencies, f_1 and f_2 close to each other, a rectangular DRA with wideband characteristic can be accomplished. Considering a DRA with side length a, width b, and height d, and $a > b$, and dielectric constant (ε_r) as shown in Figure 2.1-1 below, the simplified procedure can be shown as follows:

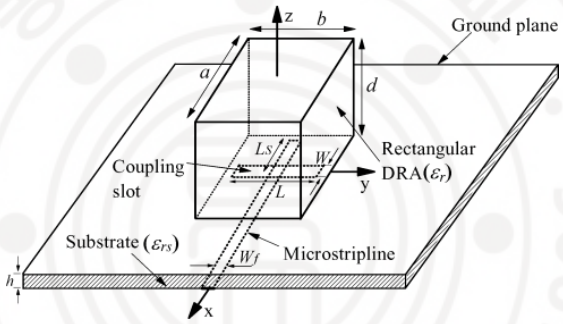

Figure 2.1-1 Configuration of a coupling slot fed rectangular DRA [44]

The frequencies f_1 and f_2 are given by:

$$f_{1,2} = \frac{c}{2\pi\sqrt{\varepsilon_r}}\sqrt{k_{x1,x2}^2 + k_{y1,y2}^2 + k_{z1,z2}^2} \tag{2.1-1}$$

Where

$$k_{y1,y2} = \sqrt{k_{1,2}^2 - k_{x1,x2}^2 - k_{z1,z2}^2} \tag{2.1-2}$$

In which the wavenumbers in the dielectric,

$$k_{1,2} = \frac{2\pi\sqrt{\varepsilon_r} f_1 f_2}{c} \tag{2.1-3}$$

And c being the speed of light in vacuum.

Then, initial values of a and d can be found as follows:

$$d_0 = \pi\sqrt{\frac{2}{k_2^2 - k_1^2}} \tag{2.1-4}$$

$$a_0 = \frac{10.32}{\sqrt{9k_1^2 - k_2^2}} \tag{2.1-5}$$

Whereby the wavenumbers can be written such as:

$$k_{x1} = k_{x2} = \frac{\pi}{a}, k_{z1} = \frac{\pi}{d}, k_{z2} = \frac{3\pi}{2d} \tag{2.1-6}$$

From here, the initial dimensions of width b can be determined based on the following DWM equation:

$$b_{1,2} = \frac{2}{k_{y1,y2}} \tan^{-1} \sqrt{\left(1 - \frac{1}{\varepsilon_r}\right)\left(\frac{k_{1,2}}{k_{y1,y2}}\right)^2 - 1} \tag{2.1-7}$$

Where b_1 and b_2 are widths of DRA at f_1 and f_2 respectively. By using curve-fitting techniques, correction terms of Δd and Δa are introduced to obtain the final dimensions of d and a:

$$\Delta d = \left[0.1393\left(\frac{f_2}{f_1}\right)^4 - 2.3209\left(\frac{f_2}{f_1}\right)^3 + 11.4422\left(\frac{f_2}{f_1}\right)^2 - 23.4984\left(\frac{f_2}{f_1}\right) + 18.4437 \right] (mm) \tag{2.1-8}$$

$$\therefore d = d_0 + \Delta d \tag{2.1-9}$$

$$\Delta a = 10.32^{-\left(1 - \frac{f_2}{f_1}\right)} (mm) \tag{2.1-10}$$

$$\therefore a = a_0 + \Delta a \tag{2.1-11}$$

To have a realistic solution, $b_1 = b_2 = b$ is required. Through a parameter known as weighting, $w = 0.65$, an optimal point is used to calculate the final dimensions of b:

$$b = wb_1 + (1 - w)b_2 \tag{2.1-12}$$

Aluminum Oxide (Al_2O_3) with dielectric permittivity, $\varepsilon_r = 9.8$ and loss tangent (tan δ) of 0.002 is chosen as the DR. Based on the desired frequency range, the lower and upper frequencies of 3.3 and 3.8 GHz are selected respectively and computed using MATLAB. The initial calculated dimensions are as shown in Table 2.1-1:

Table 2.1-1 Initial parameters of rectangular DRA

Parameter	Value (mm)

d	38.9
a	18.6
b	18.6

Low cost FR-4 glass epoxy of dielectric permittivity, $\varepsilon_{rs} = 4.4$ and loss tangent (tan δ) = 0.025 along thickness h = 1.6 mm is used as the substrate. There are several types of excitation method, however aperture coupling takes the advantage of having feed network located below the ground plane, isolating radiating aperture from unwanted coupling or spurious radiation from the feed. With the calculated dimensions, a simple rectangular DRA with aperture coupling fed technique is designed and simulated using HFSS to verify its resonance frequency.

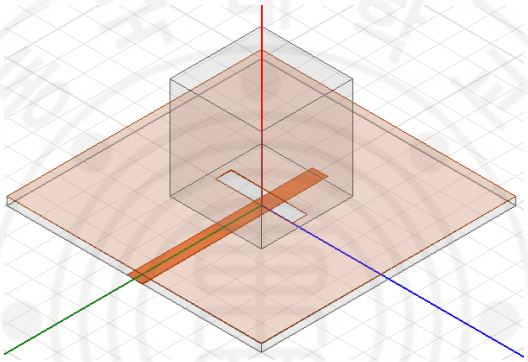

Figure 2.1-2 HFSS Simulation model of conventional rectangular DRA

For the tuned dimensions of $a = b = 18$ mm and $d = 20$ mm, the simulated reflection coefficient can be plotted in the Figure 2.1-3. Feedline, stub and aperture dimensions are estimated from [45].

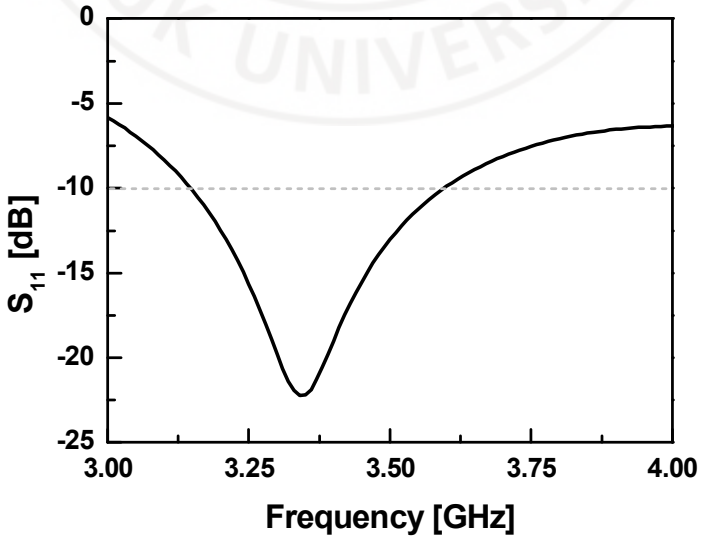

Figure 2.1-3 Reflection coefficient (S_{11}) of conventional DRA

The simulation results show a –10 dB reflection coefficient from 3.15 to 3.55 GHz, centered at 3.3 GHz.

2.2 Circular Polarization using Cross-ring Slot Structure & Truncation Feature

Circular polarization through coupling slot unequal lengths which couples the electromagnetic energy from feed line to the radiating microstrip or DR entities is first demonstrated by Huang et. al. in 1999 [46]. The cross-slot arms are placed 45° with respect to the microstrip feed line, through proper adjustment to the both arm's length ratio, fundamental resonant frequency of microstrip patch can be separated into two near-degenerate resonant modes with close to identical amplitudes and 90° phase difference.

The proposed DRA's geometry is drawn in Figure 2.2-1. FR-4 epoxy (ε_{rs}=4.4) substrate was used with thickness h of 1.6 mm, designed with an area of 46 × 46 mm^2. A ground plane was placed on top of the substrate containing the cross-ring slot arm lengths l_1 and l_2, slot radius r and width w_s, and. A rectangular shaped Al_3O_2 DR containing dimensions of $a \times b \times d$ was positioned on top of the cross-ring slot. Then, the DR was truncated at two diagonal edges at 45° with depth d_2 and length t. A 25 mm long 50-Ω MSTL of width w_f and additional stub length l_{st} is printed on the other side of the substrate.

A modified cross-slot structure with wideband AR performance is presented in [23] for 2.45 GHz. However, detailed design procedure was not provided. The proposed cross-ring slot can be designed by first determining the ring slot, following by the slot arms. The annular slot design can be predicted by referring to [47], providing a starting point before parametric optimization:

$$f_{slot} \approx \frac{c}{2\pi\left(r+\frac{w_s}{2}\right)\sqrt{\varepsilon_{eff}}} \tag{2.2-1}$$

$$\varepsilon_{eff} = \frac{\varepsilon_{rd}+\varepsilon_{rs}}{2} \tag{2.2-2}$$

whereby c is the light speed in free space. Dimensions of the innermost ring-slot with radius r along width w_s were optimized further after incorporating the slot arms with lengths l_1 and l_2. The slot arms with the same width of the ring slot were placed at 45°, 135°, 225° and 315° respectively. Initially, dimension of slot arms l_1 and l_2 can be approximated from the [45]:

$$2l_1 = 2l_2 \approx \frac{0.4\lambda_0}{\sqrt{\varepsilon_{eff}}} \tag{2.2-3}$$

Note that the ratio of the slot arms l_2/l_1 was set to 2.236 after optimization. Initial simulations are performed to determine the circular polarization of the rectangular DR excited by the cross-ring slot. Truncation width t and depth d_2 of the DR was optimally selected to achieve wider CP operation. Simulated minimum ARs are found to be resonating at 3.45 GHz and 3.80 GHz.

Finally, the designed DR and the cross-ring slot structure is merged by placing the DR on top of the cross-ring slot. The parameters are optimized accordingly as depicted in the Figure 2.2-1.

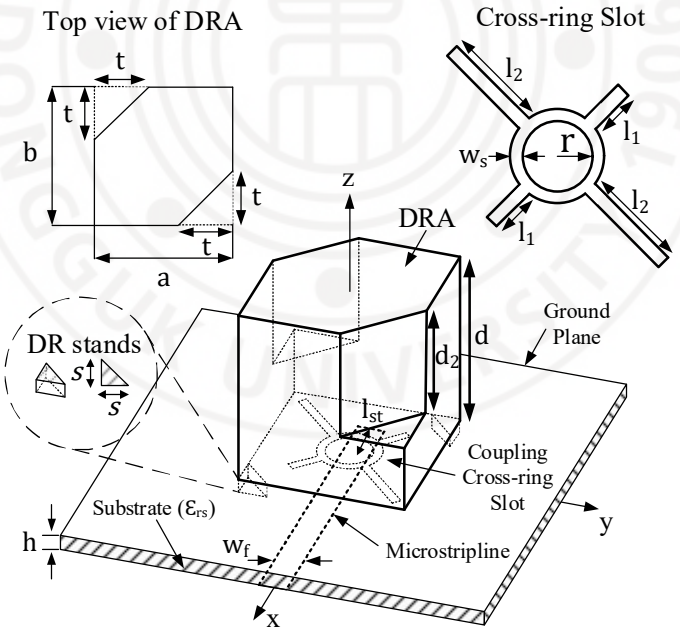

Figure 2.2-1 Geometry of proposed CPDRA

The final geometrical dimensions of the proposed CPDRA can be obtained from Table 2.1-1 below.

Table 2.2-1 Geometrical dimensions of proposed CPDRA

Variable	Value (mm)	Variable	Value (mm)	Variable	Value (mm)
$a=b$	18	s	3	w_s	1
d	20	l_1	3.3	l_{st}	7
t	7	l_2	7.38	w_f	3
d_2	12.5	r	2.5		

Figure 2.2-2 shows the E-field of the proposed DRA at 3.45 GHz, which resembles similarity to the TE_{111} mode of a regular rectangular DRA. Thus, we call this quasi-TE_{111} mode [24]. Circular polarization of the proposed antenna is verified by computing the electric field distribution on the DR at 90° phase intervals, as shown in Figure 2.2-2. Identical electric field distributions were observed at the upper CP band at 3.80 GHz caused by the dielectric-loaded cross-ring slot antenna. It was justified by the electric field distribution at the most adjacent broadside mode where the quasi-TE_{113} of the DRA at 5 GHz.

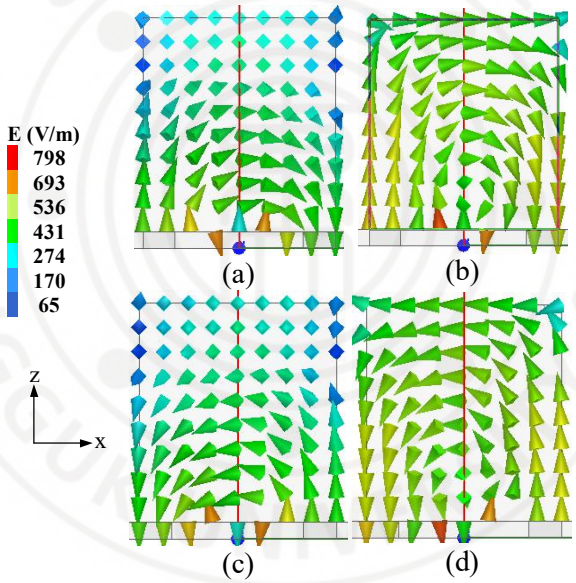

Figure 2.2-2 E-fields of the proposed DRA excited in the fundamental mode at 3.45 GHz: (a) phase 0°, (b) phase 90°, (c) phase 180°, and (d) phase 270°

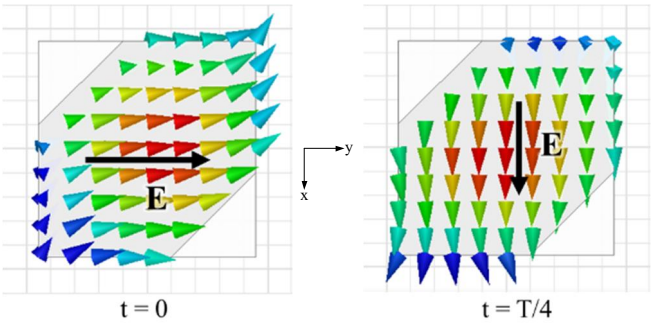

Figure 2.2-3 Figure 2.2-3 E-field distribution at the top of the DR for time period T at 3.45 GHz

The orientation of the circular polarization can be defined from the E-field vector distribution on the topmost surface of the DR (θ=0°) at 3.45 GHz, as depicted in Figure 2.2-3. For t=0, vector E points towards right, while at T/4, the vector E electric field rotates 90° clockwise as indicated in the black arrows. The two vectors are seen orthogonal to one another with clockwise rotation, hence confirming that the proposed DRA exhibits left-handed circular polarization (LHCP) radiation.

2.3 Parametric & Design Optimization

One method to produce circularly polarization for square patch antennas is by perturbation of the patch shape, which leads to the generation of two orthogonal modes with a ±90° phase difference. By truncating the opposite corners of the patch, LHCP or right -handed (R)HCP can be achieved with a typical narrowband AR performance of 1−2%. Similarly, corner truncation on the DRA can also generate CP fields in a narrow band as demonstrated by [24].

The performance of the DRA was compared with a reference antenna which is rectangular DRA with identical parameters along with the same coupling cross-slot, as portrayed in Figure 2.3-1.

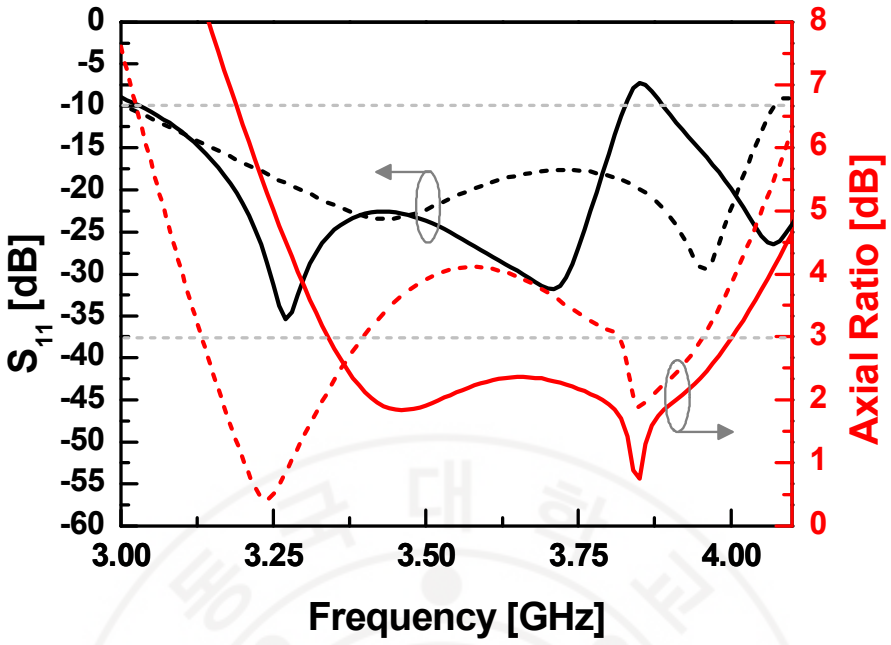

Figure 2.3-1 Simulated reflection coefficients and AR response for the proposed DRA vs. rectangular DRA as reference antenna. Solid line: proposed truncated DRA and dashed line: rectangular DRA with identical cross-ring slot excitation

Figure 2.3-1 portrays the simulated S11 and AR response of the proposed truncated DRA. In the simulation, the proposed truncated DRA demonstrated an impedance bandwidth of 0.81 GHz (3.02 – 3.83 GHz) and the 3-dB bandwidth of the antenna AR in boresight direction (θ=0°) was 0.68 GHz, ranging from 3.34 to 4.02 GHz. In contrast, the rectangular DRA has an impedance bandwidth of 1.06 GHz, ranging from 3.01 to 4.07 GHz. Although the impedance bandwidth (VSWR=2:1) is wider than the truncated DRA, the AR is significantly affected with its bandwidth shifted down to 0.27 GHz (3.14 – 3.41 GHz). Parametric study was carried out to optimize the CP performance and the impedance bandwidth of the DRA by varying the truncation parameters, cross-ring slot arm lengths, and the DR dimensions accordingly. Simulations were performed by modifying one design variable at a time while the rest remain constant.

2.3.1 DR Truncation Depth d_2 and Length t

The length t and depth d_2 of the truncation were optimally determined through the parametric analysis via 3D EM simulation (HFSS). Truncation width t was initially set to be one-third of the DR width, a (or b), and the depth d_2 was chosen as half of the DR height d before optimization.

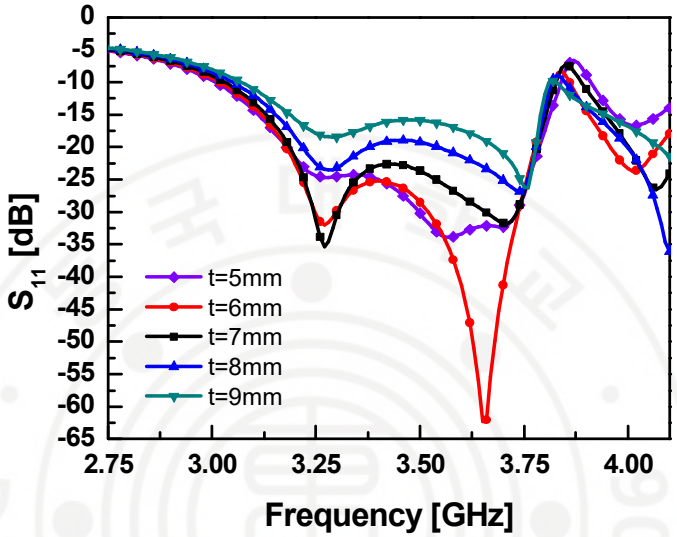

Figure 2.3-2 Simulated reflection coefficient of the proposed DRA vs. frequency for different truncation lengths (t)

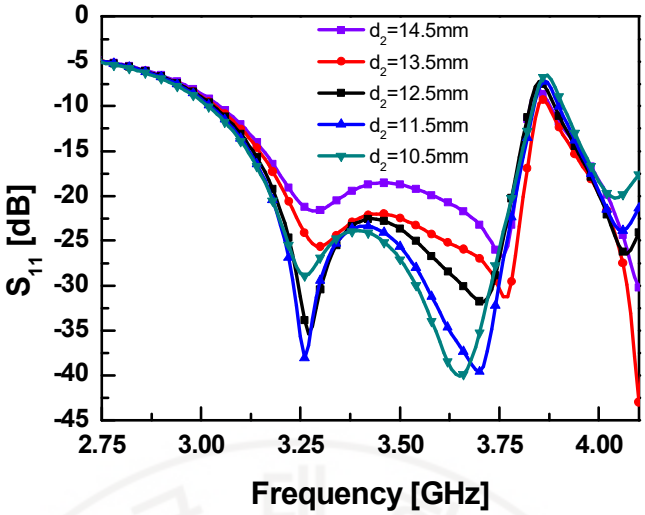

Figure 2.3-3 Simulated reflection coefficient of the proposed DRA vs. frequency for different truncation depths (d_2)

Figure 2.3-2 portrays the simulated S_{11} of the DRA versus frequency for various truncation lengths (t; 5−9 mm with 1 mm intervals). Since the antenna impedance is mainly affected by the coupling structure, there is no visible change in the impedance bandwidth for the different truncation lengths. Figure 2.3-3 presents the simulated S_{11} of the DRA versus frequency for various truncation depths (d_2; 10.5−14.5 mm in 1 mm increments). No significant change in impedance bandwidth was observed.

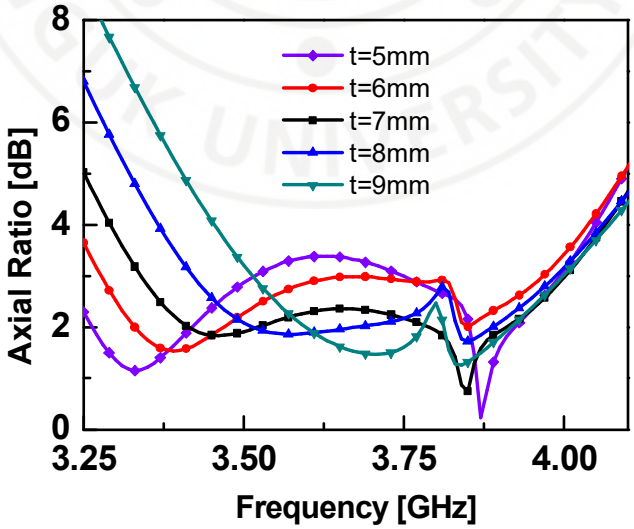

Figure 2.3-4 Simulated AR of the proposed DRA vs. frequency for different truncation lengths (t)

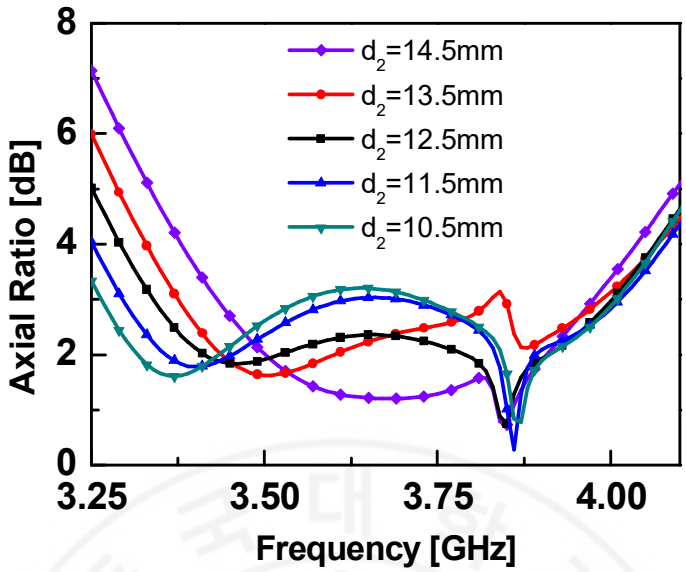

Figure 2.3-5 Simulated AR of the proposed DRA vs. frequency for different truncation depths (d_2)

On the contrary, quality of polarization performance was significantly affected by the truncation depth d_2 and length t. Figure 2.3-4 shows the corresponding AR response as a function of the truncation length t in 1 mm increments, and from the simulation, t = 7 mm is chosen to achieve broadband 3-dB AR bandwidth. The truncation depth of the DR plays an essential role in the circular polarization performance as well. As shown in Figure 2.3-5, the larger the depth, the narrower the bandwidth, although at a smaller depth, the AR at the dimensions, a truncation depth of 12.5 mm gave the widest 3-dB AR bandwidth.

2.3.2 Slot-arms Lengths l_1 and l_2

In Figure 2.3-6, the simulated reflection coefficient of the proposed DRA versus frequency for different slot-arm lengths (l_1 from 2.3−2.4 mm at 0.5 mm intervals while l_2 was kept fixed at 7.38 mm). As can be seen, the resonant frequency shifted down at longer lengths with dramatic changes in the impedance bandwidth. However, in Figure 2.3-7, the simulated ARs are presented depending on the l_1 slot-arm length with the same dimension variations. In a seemingly opposite manner, the desirable CP happened at lower frequency with shorter l_1 slot-arm length.

Optimal impedance and AR bandwidth at the designated frequency range could be obtained with l_1 = 3.3 mm. The AR performance for the different slot-arm l_2 lengths (6.38−8.38 mm with 0.5 mm, intervals while keeping l_1 fixed at 3.3 mm). The AR performance for the same slot-arm l_2 variation is shown in Figure 2.3-9. It was found that the impedance bandwidth widened with a shorter length of l_1 (Figure 2.3-8). Similarly, the AR with shorter lengths had a narrower bandwidth. Above a certain length, weak CP with AR larger than 3 dB is observed. For l_2 = 7.38 mm, the bandwidth of the 3-dB AR was the widest among the parametric analysis results.

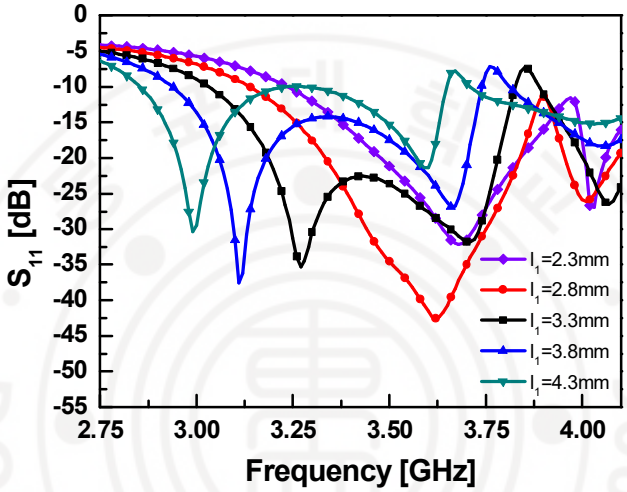

Figure 2.3-6 Simulated reflection coefficient of the proposed DRA vs. frequency for the different l_1 slot-arm lengths

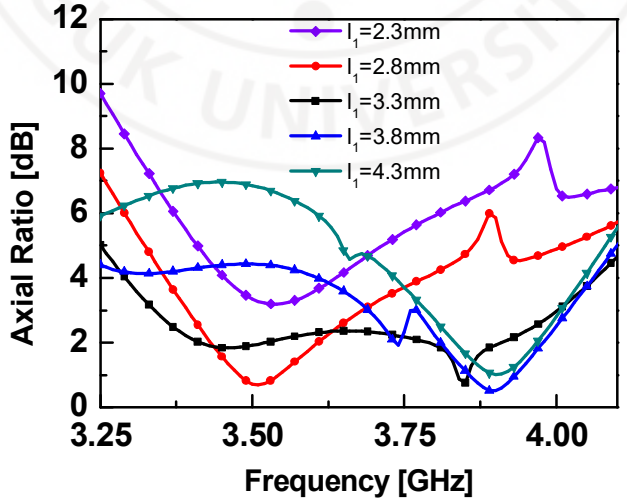

Figure 2.3-7 Simulated AR of the proposed DRA vs. frequency for the different l_1 slot-arm lengths

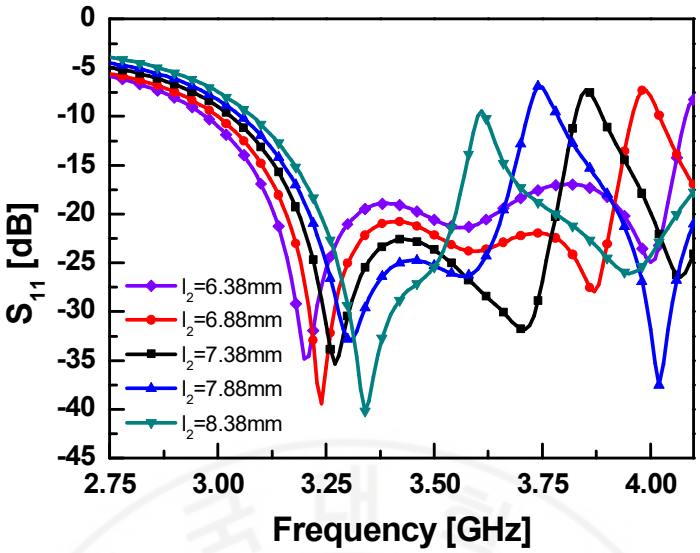

Figure 2.3-8 Simulated reflection coefficient of the proposed DRA vs. frequency for the different l_2 slot-arm lengths

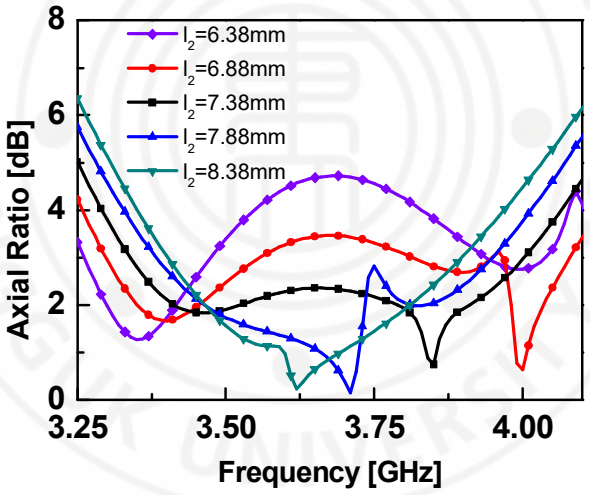

Figure 2.3-9 Simulated AR of the proposed DRA vs. frequency for the different l_2 slot-arm lengths

2.3.3 DR Height, *d*

Figure 2.3-10 displays the simulated return loss of the DRA against frequency for various DR heights (d; 18−24 mm), which confirmed that there was no visible degradation in the impedance bandwidth. The AR in Figure 2.3-11 shows the quality of CP strongly affected by the DR height (d): the AR improved until d = 21 mm. However, as d became larger, this severely degraded the AR (quite close to 4 dB at

3.85 GHz). Therefore, the best AR response could be obtained with d = 20mm for the aimed 5G communication applications (3.3 – 3.8 GHz).

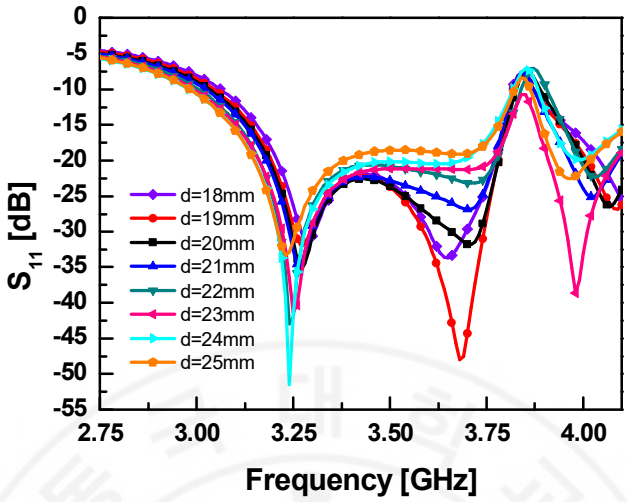

Figure 2.3-10 Simulated reflection coefficients of the proposed DRA vs. frequency for different DR heights (d)

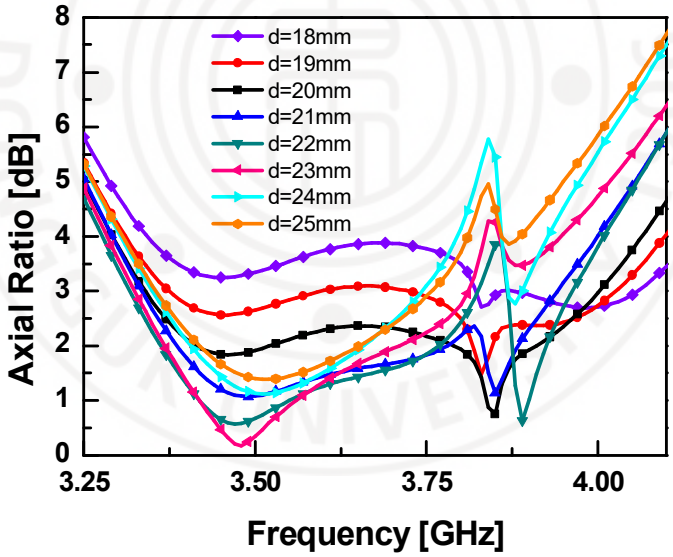

Figure 2.3-11 Figure 2.3.3-2 Simulated AR of the proposed DRA vs. frequency for different DR heights (d)

2.3.4 DR Side Length, *a*

Figure 2.3-12 displays the simulated return loss of the DRA against frequency depending on the DR side length (a; 16−20 mm). S_{11} changed abruptly at a = 19mm, while a = 20, a much wider impedance bandwidth was attainable. However, the AR

response was severely degraded to nearly above 7 dB at around 3.8 GHz, as shown in Figure 2.3-13. Hence, the optimal DR side length was chosen as a = 18 mm.

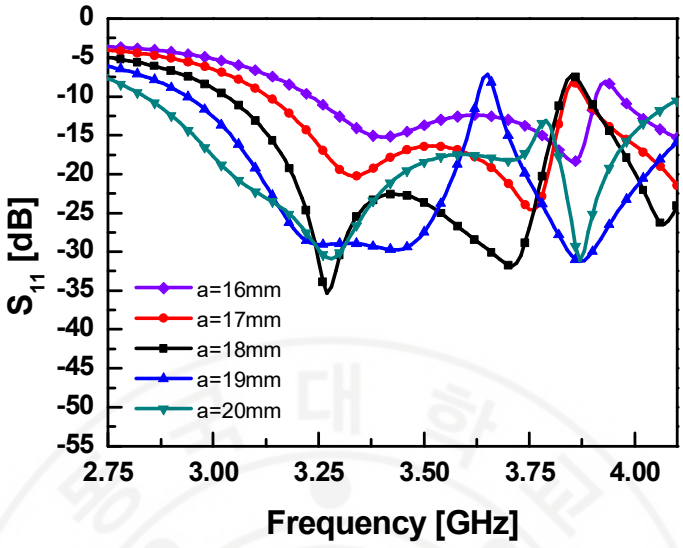

Figure 2.3-12 Simulated reflection coefficients of the proposed DRA vs. frequency for DR side lengths (a)

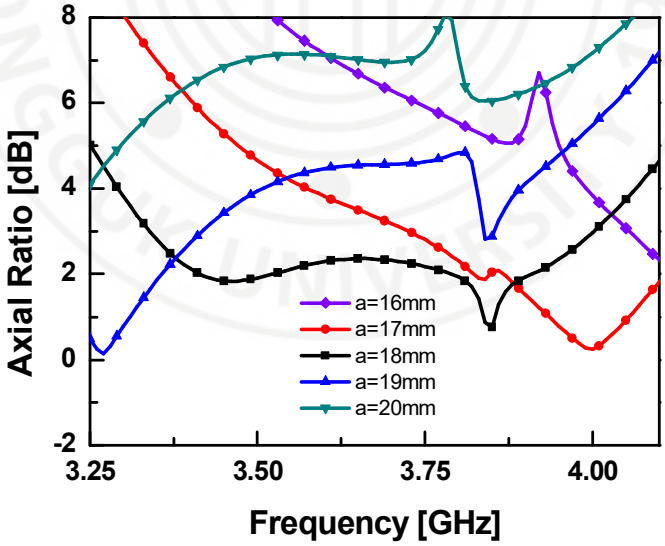

Figure 2.3-13 Simulated AR of the proposed DRA vs. frequency for DR side lengths (a)

2.4 Effect of Adhesive

DRs are typically mounted on the substrate with a feed structure along with the ground plane using adhesive solution. Antenna impedance and quality of polarization are among the radiation characteristics commonly influenced by the extra layer of adhesive, primarily due to mismatch between the different permittivity of the nonzero thickness adhesive layer [48], [49]. Therefore, the adhesive must be precisely accounted for during the design stage to predict the realized DRA performance. In [48], spin coating was applied on the edges of the DR and substrate, incurring some machinery expense. Even though no adhesive was used in [49], a strategic hole was drilled into a secondary ground plane to place the DR with two identical metal holder pins soldered beside the hole for precise positioning, which increases the fabrication difficulty to a certain degree. For this specific case, there has not been an efficient design to avoid this issue yet.

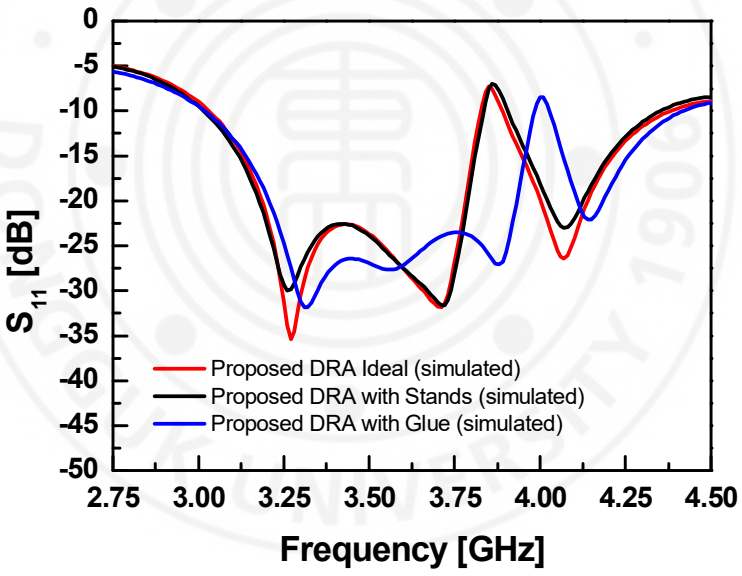

Figure 2.4-1 Comparison of S_{11} of the proposed antenna mounted using miniature stands and with adhesive

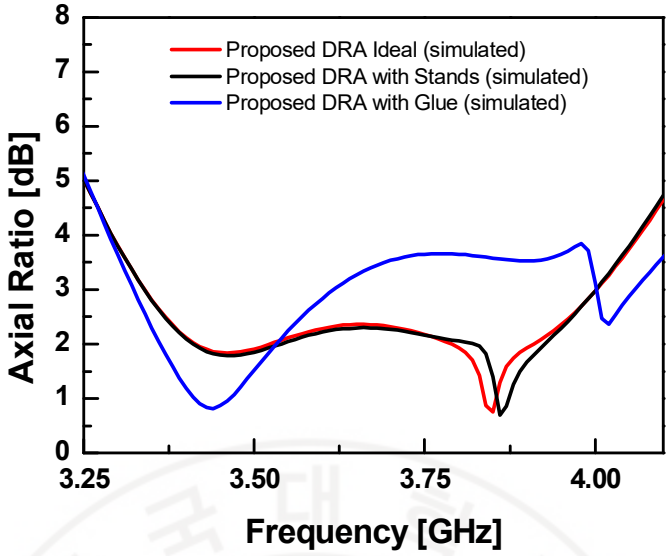

Figure 2.4-2 Comparison of AR of the proposed antenna mounted using miniature stands and with adhesive

To gauge the effects of an ordinary adhesive, the S_{11} and AR performance between a DRA mounted with glue and one with small triangular stands is compared. The simulated reflection coefficient and AR performance are displayed in Figure 2.4-1 and Figure 2.4-2, respectively. The DRA ideally placed on top of the substrate is carried out without any glue. A layer of glue with an estimated dielectric permittivity of 3.65 at 3.5 GHz (extracted from results in [50]) was simulated with a thickness of 0.05 mm. By applying the layer of glue, simulated reflection coefficient widened from 3.02 to 3.98 GHz whilst the AR bandwidth severely degraded over the designated operation band. The thin layer of glue significantly affects the circular polarization of the DRA due to the additional dielectric permittivity, causing unwanted changes in radiation characteristics. To avoid performance degradation due to adhesive, short triangular posts are included at the bottom side of the DR to physically mount the DR to the printed circuit board (PCB) instead.

The simulated results of the ideal case with no adhesive and the proposed DRA with triangular stands at the bottom of DR exhibits no differences in reflection coefficient, AR performance, and radiation pattern.

Chapter 3 MEASUREMENT RESULTS & DISCUSSION

3.1 Fabrication and Radiation Pattern Measurement of Proposed CPDRA

The DR made of alumina ceramic is fabricated through a laser machining vendor and the substrate is etched using the LPKF PCB milling machine. The figure below illustrates the prototype of the CP-DRA.

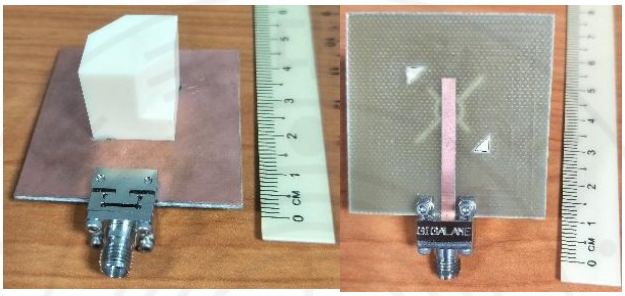

(a) (b)

Figure 3.1-1 (a) top view (b) bottom view

The radiation pattern, inclusive of AR of the proposed CPDRA were measured in an anechoic chamber at three frequency points covering the center, lower, and upper frequencies of the designated frequency range (Figure 3.1-2(a)). The chamber was installed with a near-field scanner along a far-field tower to assess the radiation pattern of the proposed CPDRA. The radiation patterns were measured at 3.45, 3.65 and 3.8 GHz, which overlaps the center, lower and upper frequency points of the desired operation band. The radiation pattern was measured at 1-degree step interval in the anechoic chamber having range of 0−360°. The reflection coefficients of the proposed DRA, rectangular DRA, and the DRA with a thin glue later were measured with an N5224A PNA Network Analyzer, as depicted in Figure 3.1-2(b).

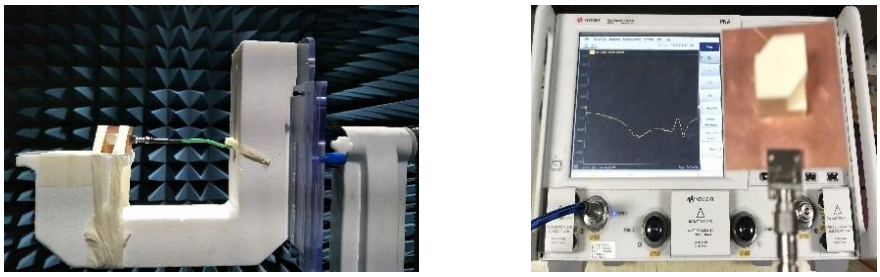

(a) (b)

Figure 3.1-2(a) Measurement setup for (a) radiation pattern and axial ratio (AR) and (b) antenna input impedance versus frequency

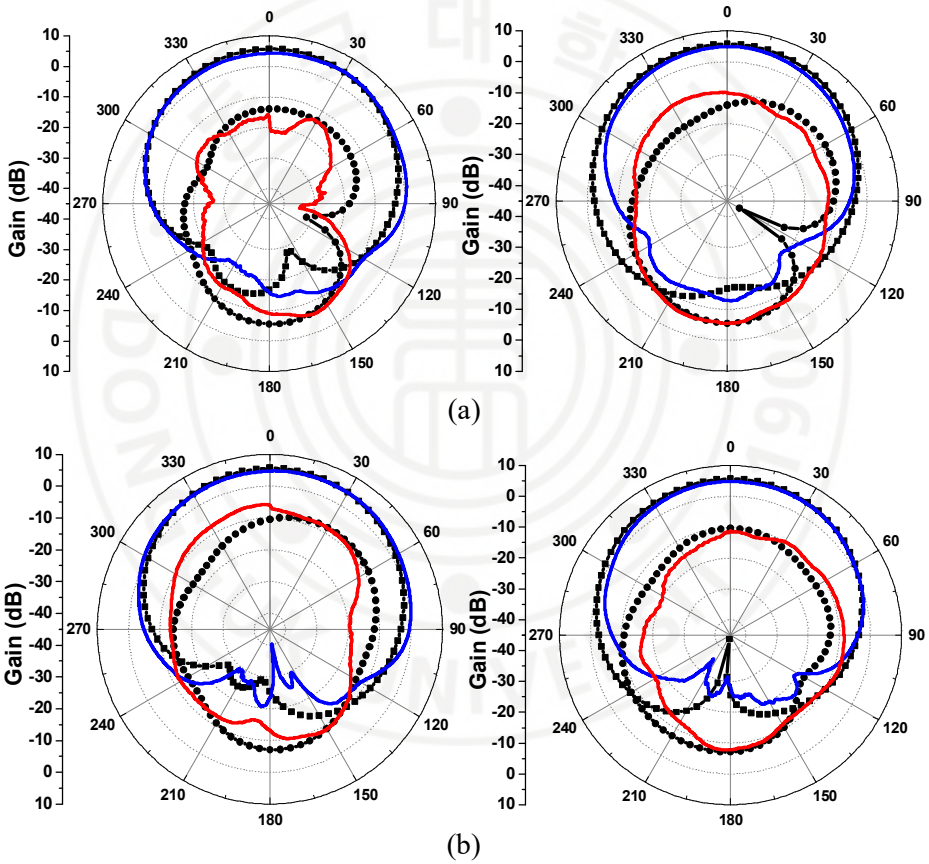

(a)

(b)

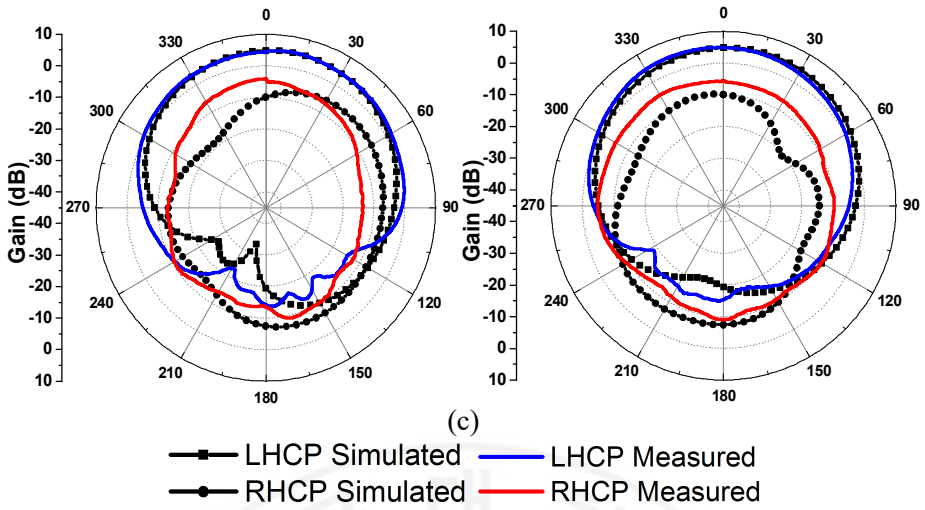

Figure 3.1-3 Radiation patterns of the proposed DRA at (a) 3.45 GHz, (b) 3.65 GHz and (c) 3.80 GHz (x-z plane images on the left-hand side and y-z plane images on the right-hand side)

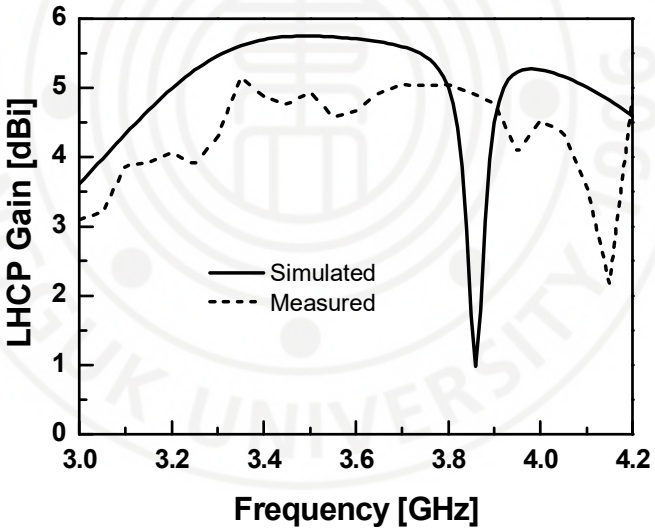

Figure 3.1-4 Measured and simulated LHCP gain of the proposed CPDRA

Figure 3.1-3 shows the simulated radiation patterns of the DRA in x-z (Φ=90°) and y-z planes (Φ=0°) at 3.45, 3.65 and 3.80 GHz, respectively. In the boresight, LHCP gain is greater than RHCP by approximately 19, 17 and 18 dB at 3.45, 3.65 and 3.80 GHz, which validates that the DRA exhibit LHCP radiations. Figure 3.1-4 portrays the simulated and measured gain plot of the proposed antenna. A peak gain

of 4.83 dBi is measured within the designated frequency band of the antenna is attained. It is known that the measured gain is typically lesser than the simulated result as experiment imperfections such as connectors and cables losses are not included in the far-field measurements.

3.2 Reflection Coefficient and Axial Ratio

The proposed truncated DRA demonstrated simulated and measured impedance bandwidths (S_{11}) of 23.7% and 25.9% (of VSWR=2:1) from 3.02 to 3.83 GHz and 3.06 to 3.97 GHz frequency range respectively, shown in Figure 3.2-1. The simulated and measured axial ratio (AR) bandwidths of the antenna were 18.5% ranging from 3.34 to 4.02 GHz and 18.7% from 3.15 to 3.80 GHz in the boresight path (θ=0°), as presented in Figure 3.2-2. In contrast, the rectangular DRA had simulated and measured impedance bandwidths of 29.5% from 3.01 to 4.07 GHz, and 32% from 2.97 to 4.12 GHz. The simulated AR for the rectangular DRA was 8% from 3.11 GHz to 3.37 GHz. The measured results of the AR for the reference rectangular DRA showed similar trend to the value larger than 3 dB from 3.5 to 3.95 GHz, which indicates that the truncation dramatically enhanced the CP performance. The frequency shifted downward slightly in the AR response of the proposed CPDRA due to incomplete physical contact between the antenna ground plane and the DR during fabrication, resulting in an uneven air gap. Another highly probable reason would be that the platform support with tape binding of the DRA during measurement in the anechoic chamber contributed towards the effect on radiation pattern resulting a wider AR in the experiment. In contrast, simulation performed is always calculated under ideal conditions [51].

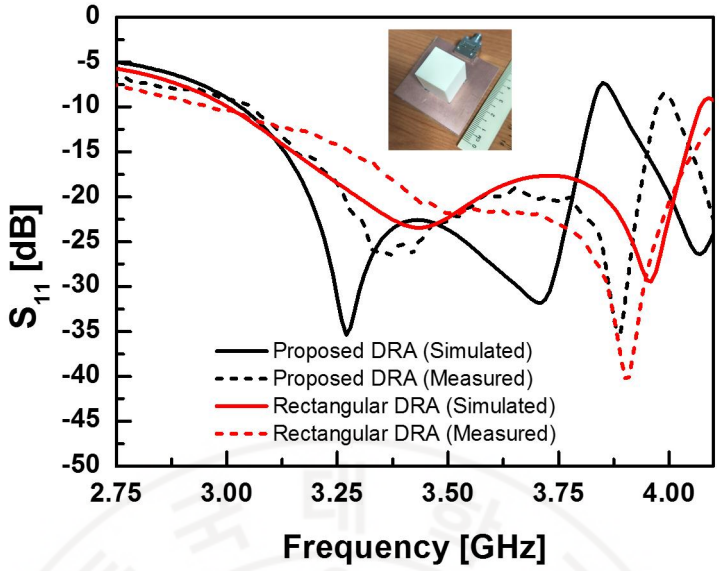

Figure 3.2-1 Comparison of reflection coefficients of the proposed DRA with truncation and the rectangular DRA

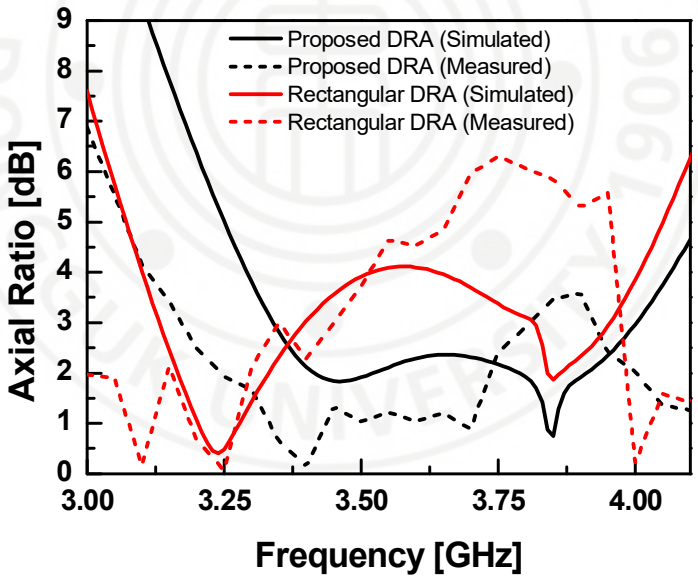

Figure 3.2-2 Comparison of AR of the proposed DRA with truncation and the rectangular DRA

The CPDRA with the applied glue layer was also investigated. The simulated and measured impedance bandwidths are 27.4% ranging from 3.02 to 3.98 GHz and 30% from 3.3 to 4.48 GHz, respectively, as shown in Figure 3.2-3. The AR response

displayed a narrower bandwidth of 8% (3.33 to 3.61 GHz) in simulation results and 7% (3.40 to 3.65 GHz) in measurement as depicted in Figure 3.2-4.

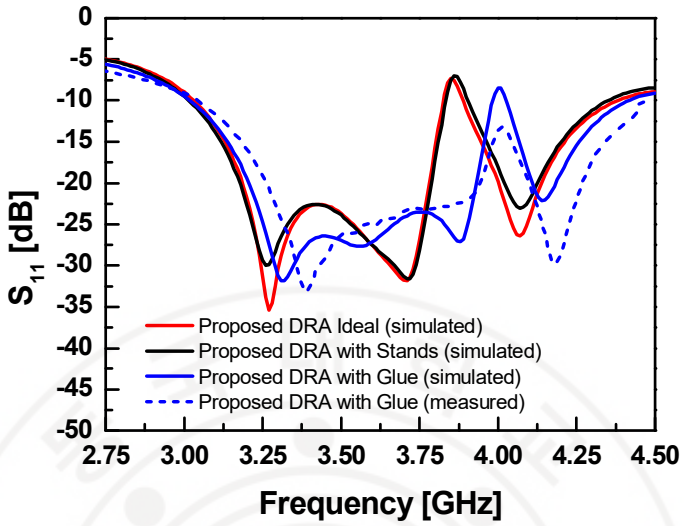

Figure 3.2-3 Comparison of S_{11} of the proposed antenna mounted using triangular stands and with glue

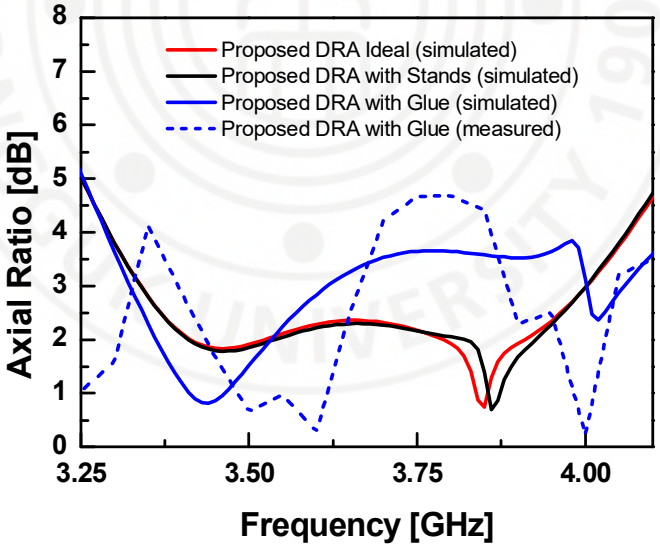

Figure 3.2-4 Comparison of AR of the proposed antenna mounted using triangular stands and with glue

3.3 Comparison with State-of-the-Art Designs

Table 3.3-1 lists the comparison of the proposed CPDRA and existing singly fed CPDRAs. Different CP excitation methods, DR types, center frequency, dielectric permittivity of DR were included for design technique comparison. Parameter of DR height is listed for vertical DR size comparison, which is the main concern for wireless communication systems. Appended in the final two columns, AR bandwidth and LH(RH)CP gain are solely aimed at performance comparison. Measured results are presented in the mentioned table accordingly to verify the practical performance of the proposed single element CPDRA.

At a glance, the proposed CPDRA demonstrates a relatively extensive AR bandwidth compared to previously reported designs. Furthermore, the gain is considerably above average.

Table 3.3-1 Performance comparison of proposed CPDRA design with the sate-of-the-art designs in the literature

Ref.	CP Excitation Method	DR Type	[a]f_0 (GHz)	ε_{rd}	DR Height (mm)	[b]BW_{AR} (%)	LH(RH)CP Gain (dBi)
[15]	Rectangular aperture	Stair-shaped	10	12	0.15 λ_0	10.2	-
[16]	Strips	Hollow Rectangular	2.41	9.4	0.18 λ_0	12.4	6.44
[17]	Spiral strip	Rectangular	4.26	9.3	0.36 λ_0	7	4
[18]	Inclined slots with parasitic strips	Slotted	3.6	15	0.29 λ_0	25	1.48
[19]	Inclined slots with probe	Hollow rectangular	2.5	10	0.26 λ_0	7.3	1.6
[22]	Cross slot fed with cross tuning stub	Rectangular	1.268 & 1.561	20.5	0.23 λ_0	2.9 & 2.4	5.5 & 4.5
[24]	Rectangular slot with DR truncation	Truncation with center groove	1.58 & 2.44	9.8	0.21 λ_0	6.3 & 3.68	6.09 & 8.49
[26]	Circular ring feed with (+)-shaped slot	Rectangular	3.37	9.8	0.20 λ_0	12.03	5
[61]	Modified CPW feed with slotted patches	Half-split cylindrical	4.75	9.8	0.18 λ_0	17.34	1.56
[62]	Concentric parasitic half-loops	Rectangular	3.2	9.2	0.27 λ_0	13	5
[63]	Rectangular slot with Dual-offset feed line	Pixelated	3.2	9.8	0.33 λ_0	14.63	6.13
This Work	**Cross-ring slot with DR truncation**	**Partial truncation**	**3.45**	**9.8**	**0.23 λ_0**	**18.7**	**4.83**

[a]Operating frequency; [b]Bandwidth of 3dB axial ratio

Chapter 4 MIMO CONFIGURATION

By etching the electromagnetic bandgap (EBG) structure onto the ground plane of the microstrip line used in the antenna, the proposed DRA with array configuration can accomplish improved diversity performance without extra area consumption. In the following section, geometry and analysis of the CPDRA MIMO configuration along with the EBG structure will be discussed accordingly.

4.1 Electromagnetic Band-gap Unit Cell

Electromagnetic bandgap (EBG) is a periodic structure commonly used in RF circuits, exhibiting frequency regions where surface wave propagation is restricted [52]. Planar EBGs having wide bandgap properties without the use of vias are investigated thoroughly in [53], [54], [55]. The characteristic of the uniplanar compact (UC-EBG) geometry is evaluated by finite element-based analysis for a single unit cell and plotting of the dispersion diagram. The optimized planar EBG structure can therefore be used to reduce mutual coupling of a MIMO antenna array.

The general length of an EBG element are known to be approximately half-wavelength [52] or $\lambda_g/2$, which is about 20 mm in this case. The design parameters of the proposed EBG unit cell are E_s = 0.572 mm, E_1 = 7.592 mm, E_2 = 5.73 mm and E_3 = 17.735 mm as portrayed in Figure 4.1-1. 3-D finite element (FEM) code with vector finite elements have been implemented to investigate the EBG dispersion diagram. A single cell is used for computations in HFSS, where periodic boundary conditions (PBC) at the surrounding cell sidewalls are imposed to imply periodicity as demonstrated Figure 4.1-2. The cell domain is then terminated with perfectly matched layers (PML) on top [55].

The EBG structure's bandgap is determined by extracting the dispersion diagram shown in Figure 4.1-3, and the bandgap region is identified as the frequency region where no mode is prohibited. The bandgap frequency range of the designed EBG is around 3.36 GHz to 4.43 GHz.

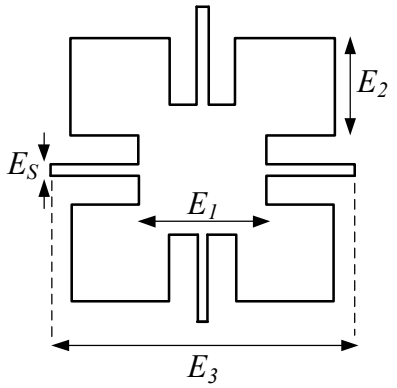

Figure 4.1-1 EBG unit cell geometry

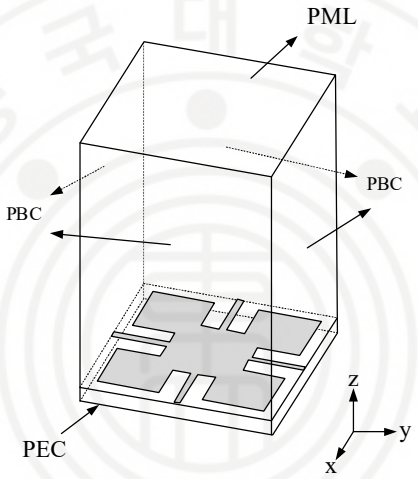

Figure 4.1-2 Model setup to simulate dispersion diagram in HFSS

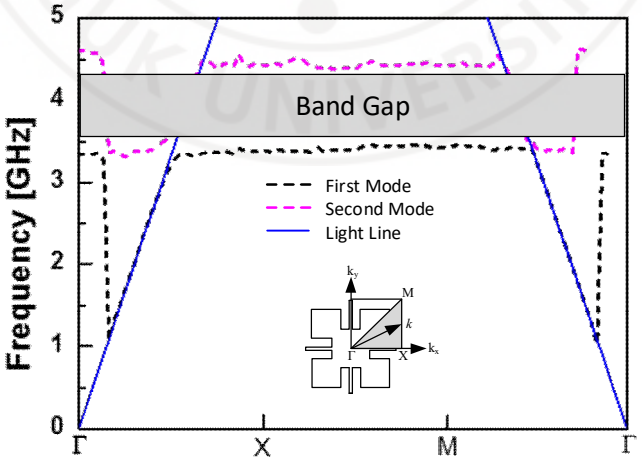

Figure 4.1-3 Dispersion diagram of EBG unit cell

4.2 Circularly Polarized MIMO DRA

The circularly polarized MIMO DRA implementing the EBG structure designed from the previous section is proposed as shown in Figure 4.2-1(a) and the fabricated antenna in Figure 4.2-1 (b). The DRAs are positioned on the substrate with 95 × 49.7mm^2 area. Center-to-center spacing is benchmark at $\lambda_0/2$, such that λ_0 is the wavelength with respect to lowest operation frequency at 3.3 GHz. The EBG unit cells are engraved onto the ground plane, with first two unit cells aligned at the center with respect to y-axis, and then extended by half a cell on the top and bottom direction. The distances and alignments of the unit cells are verified through numerous parametric analysis.

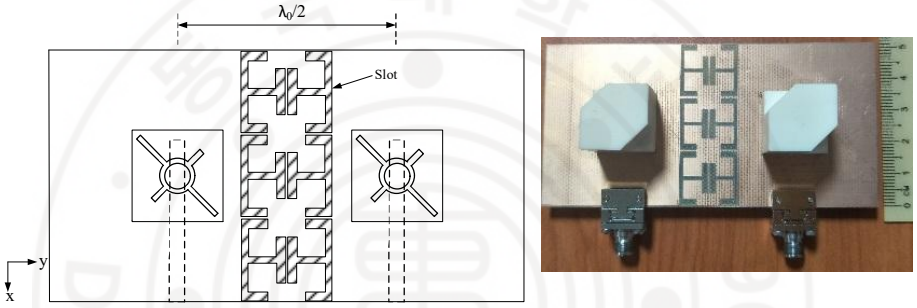

(a) (b)

Figure 4.2-1 (a) Geometry of proposed MIMO CPDRA (b) Fabricated MIMO CPDRA

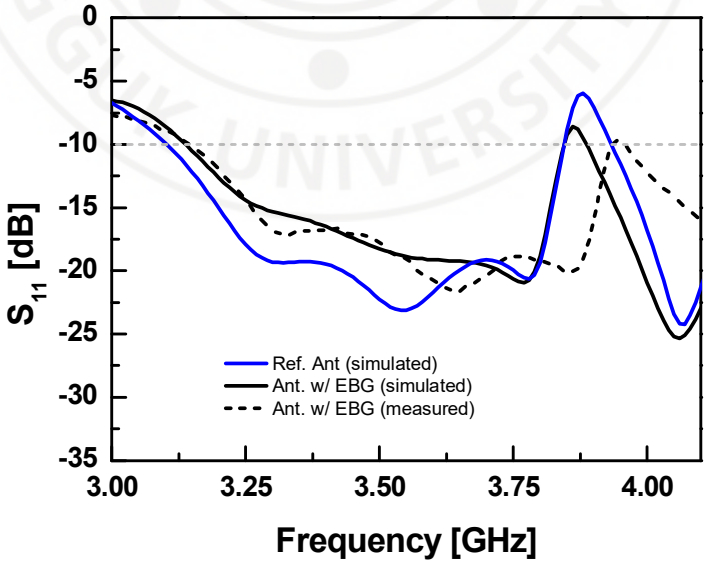

Figure 4.2-2 Comparison of S_{11} for MIMO DRA with and without EBG

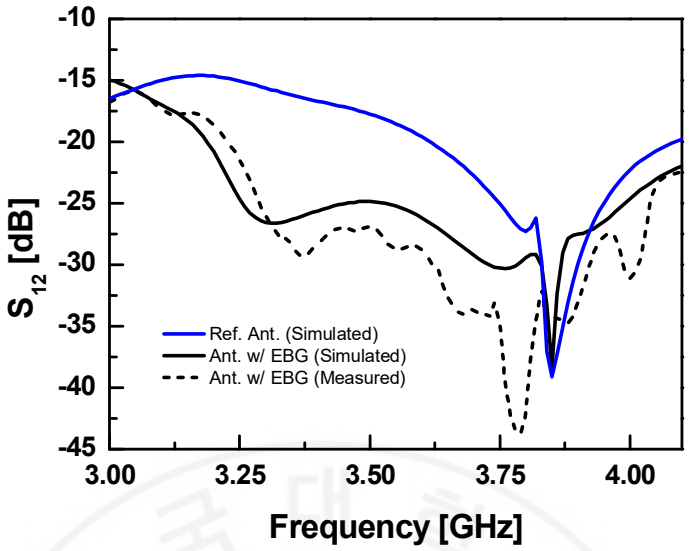

Figure 4.2-3 Comparison of S_{12} for MIMO DRA with and without EBG

Figures 4.2-2 and 4.2-3 shows the simulated and measured reflection coefficient, S_{11} along with transmission coefficient, S_{12} respectively. The performances are compared to an identical MIMO DRA design with no EBG structure, labeled as reference antenna. It can be determined from the proposed antenna with the simulated and measured S_{11} bandwidth covering frequencies 3.11 to 3.84 GHz and 3.15 to 3.93 GHz, demonstrating similar characteristics with the single CPDRA.

Furthermore, an isolation below –24 dB from simulation result and –26 dB from measurement is attained within the desired frequency band as compared to the reference antenna without EBG structure at approximately –17 dB. Comparison of surface current distribution of proposed DRA and reference antenna is performed through HFSS simulation accordingly in Figure 4.2-4. The inclusion of the EBG demonstrated lesser current flow from DRA 1 to DRA 2 when excited on an individual DRA. The analysis is carried out such that DRA 1 (left) is excited, and DRA 2 (right) is terminated by 50-Ω. Wide AR bandwidth is maintained as per single DRA configuration as shown in the AR plot in Figure 4.2-5, plotted along with comparison of with and without EBG structure. On top of that, the simulated antenna gain and radiation pattern are not affected with the applied EBG structure, as presented in Figure 4.2-6, and Figure 4.2-7, respectively.

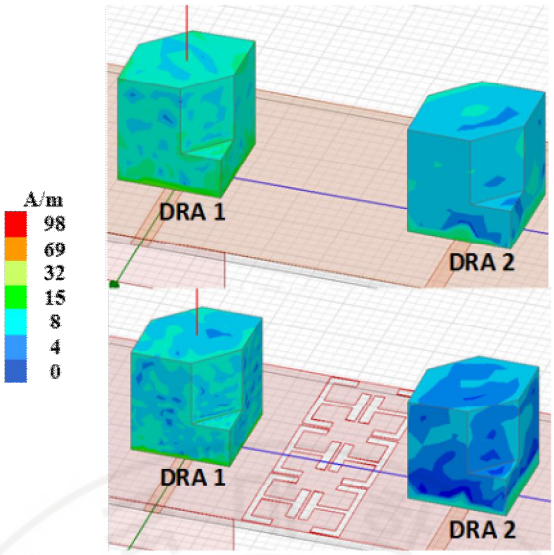

Figure 4.2-4 Comparison of MIMO CPDRA surface current distribution with and without EBG

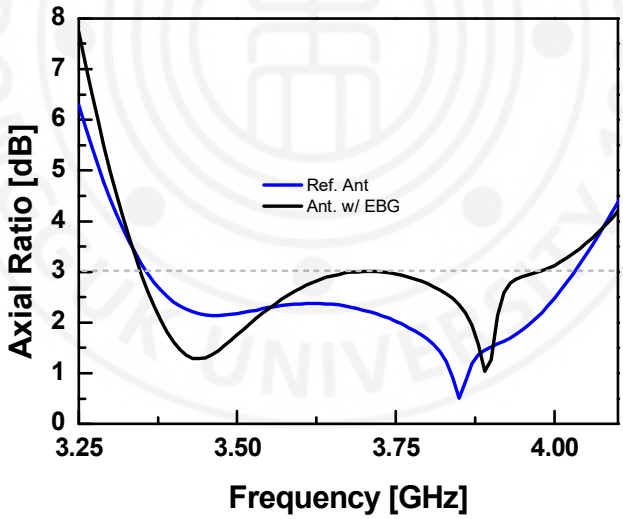

Figure 4.2-5 Comparison of MIMO CPDRA AR with and without EBG

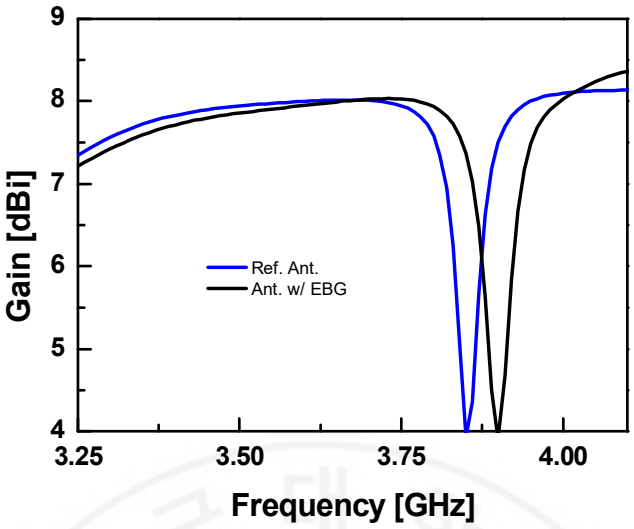

Figure 4.2-6 Gain comparison of MIMO CPDRA with and without EBG

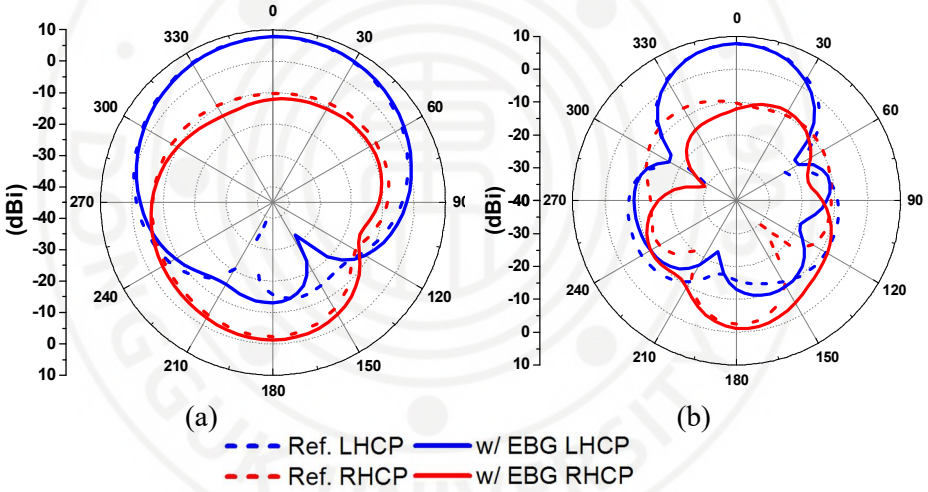

Figure 4.2-7 Two-dimensional radiation pattern for antenna with and without EBG

4.3 Antenna Diversity Analysis

Due to multipath fading, destructive interference can take place. Proper antenna diversity scheme can be taken place to counter these unwanted conditions. The proposed CP MIMO DRA can be validated through three essential figures of merit, which are envelope correlation coefficient (ECC), diversity gain (DG) and channel

capacity loss (CCL) [56] – [60] for its diversity performance. Performance comparison with state-of-the-art MIMO CPDRAs are also carried out in section 4.4.

4.3.1 Envelope Correlation Coefficient

Correlation coefficient is a critical parameter for systems exhibiting diversity. This parameter can be viewed in the aspects of complex and envelope. The complex measure of correlation between received signals at the antennas can be given as [56]:

$$\rho_c = \frac{\int_0^{2\pi}\int_0^{\pi}\left(XPRE_{\theta m}(\theta,\varphi)\mathrm{E}^*_{\theta n}(\theta,\varphi)\mathrm{P}_{\theta}(\theta,\varphi)+E_{\varphi m}(\theta,\varphi)\mathrm{E}^*_{\varphi m}(\theta,\varphi)\mathrm{P}_{\varphi}(\theta,\varphi)\right)\sin\theta d\theta d\varphi}{\sqrt{\sigma_m^2\sigma_n^2}} \tag{4.3-1}$$

where P_θ and P_φ are the angular diversity functions of the incident power with respect to θ and φ directions, σ_m^2 and σ_n^2 represents variances of m^{th} and n^{th} branches and XPR represents the cross-polarization power gain which is defined as:

$$XPR = \frac{\int_0^{2\pi}\int_0^{\pi} P_{\theta}(\theta,\varphi)\sin\theta\sin\theta d\varphi}{\int_0^{2\pi}\int_0^{\pi} P_{\varphi}(\theta,\varphi)\sin\theta\sin\theta d\varphi} \tag{4.3-2}$$

The complex correlation can be further mathematically simplified as:

$$\rho_c = \int_0^{2\pi}\int_0^{\pi}\left(XPRG_{\theta m}(\theta,\varphi)P_{\theta}(\theta,\varphi)+G_{\varphi m}(\theta,\varphi)P_{\varphi}(\theta,\varphi)\right) \tag{4.3-3}$$

For,

$$G_{\theta m}(\theta,\varphi) = E_{\theta m}(\theta,\varphi)\mathrm{E}^*_{\theta n}(\theta,\varphi) \tag{4.3-4}$$

$$G_{\varphi m}(\theta,\varphi) = E_{\varphi m}(\theta,\varphi)\mathrm{E}^*_{\varphi n}(\theta,\varphi) \tag{4.3-5}$$

where $E_{\theta m}$ and $E_{\varphi m}$ are complex electric fields in θ and φ directions respectively for the m^{th} antenna. The same equations are applicable for n^{th} antenna. The envelope correlation for a Rayleigh fading channel can be given as:

$$\rho_e = \left|\rho_c\right|^2 \tag{4.3-6}$$

The performance of MIMO antennas is measured through the envelope correlation coefficient (ECC). The ECC assesses the similarity between two antennas' radiation patterns. For an ideal case of ECC = 0, two radiation patterns do not overlap each other, incoming signal is received by any of the single array element from any

direction. On the other hand, when ECC = 1, both radiation patterns are considered identical. Thus, signal will be equally received by both ports, which is undesirable. ECC of lower values are generally preferred, whereby values lesser than 0.5 is known to be acceptable. The ECC can be calculated with the following equation in [57]:

$$ECC = \rho_e = \frac{|S_{ii}^{*}S_{ij} + S_{ji}^{*}S_{jj}|^2}{\left[1-(|S_{ii}|^2+|S_{ji}|^2)\right]\left[1-(|S_{jj}|^2+|S_{ij}|^2)\right]} \quad (4.3\text{-}7)$$

Figure 4.3-1 depicts the compared simulated and measured ECCs for the proposed antenna and reference antenna.

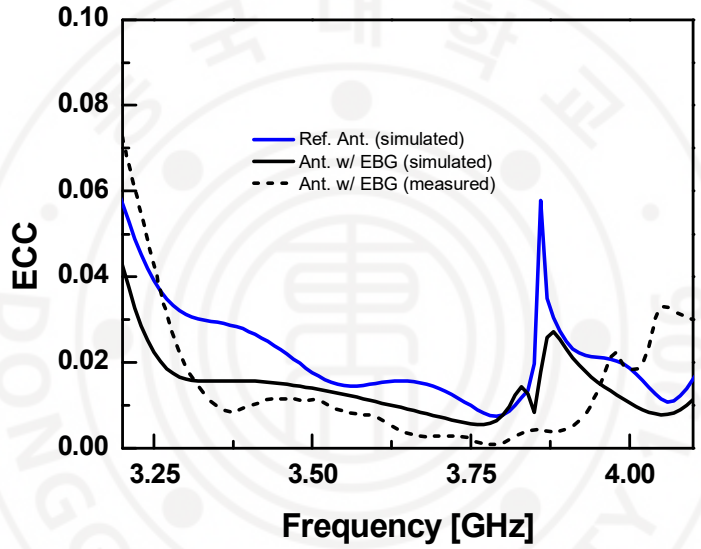

Figure 4.3-1 Comparison of envelope correlation coefficients (ECC) for antenna with and without EBG

4.3.2 Diversity Gain

Like the ECC, diversity gain (DG) is an essential parameter used to quantify diversity performance of MIMO antennas. DG is known as the slope of the error probability curve in terms of received signal-to-noise ratio (SNR) scale in a log-log scale. So, the DG can be defined as the increment of SNR at a given probability, usually around 1% or 10% [56]. In this regard, the DG is capable to be calculated in a simple manner by referring to the cumulative distribution function (CDF) curves of the SNR, and by comparing the combined SNR using specific diversity technique

with the SNR of an un-coded single-input single-output (SISO) communication system. This can be expressed by the following equation:

$$DG = \frac{(SNR)_c}{(SNR)_r} \tag{4.3-8}$$

where annotation '*c*' and '*r*' refers to combined and the reference. The theoretical relationship between ECC and DG is presented in [58]:

$$DG = 10 \times \sqrt{1 - |ECC|} \tag{4.3-9}$$

The above equation infers the lower the ECC, the higher the DG. Hence, high isolation between the antennas are required. To sum up, maximum diversity can be accomplished when the ECC is zero. In most cases, DG value of 10 is usually considered ideal. However, value above 6 is within good level [59]. As shown in Figure 4.3-2, the DG of the proposed antenna is greater than 9.8 within the operation band.

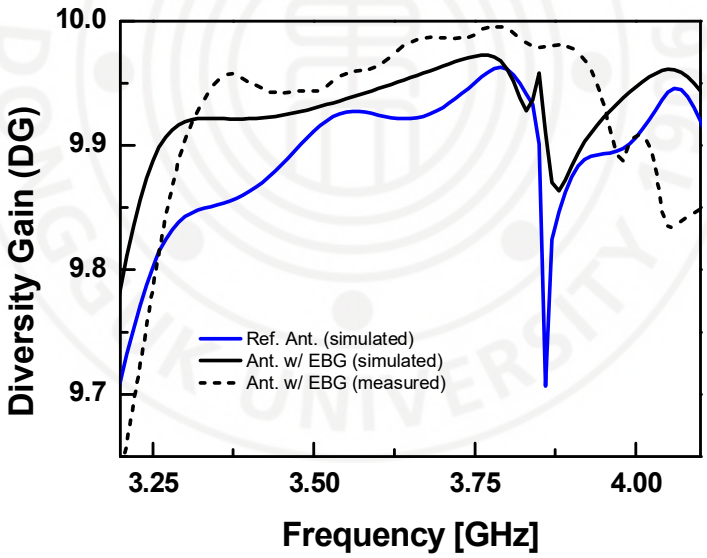

Figure 4.3-2 Diversity gain (DG) comparison for antenna with and without EBG

4.3.3 Channel Capacity Loss

Channel capacity loss (CCL) is usually affected by the coupling between various antennas in an array, such that CCL increases proportionally to the number of

antenna elements. Since correlation between array elements in a MIMO channel forms CCL, the equation can be written as below [60]:

$$CCL = -\log_2 \det\left(\psi^R\right) \tag{4.3-10}$$

$$\psi^R = \begin{bmatrix} \rho_{11} & \rho_{12} \\ \rho_{21} & \rho_{22} \end{bmatrix} \tag{4.3-11}$$

$$\rho_{ii} = 1 - \left(\left|S_{ii}\right|^2 + \left|S_{ij}\right|^2 \right) \tag{4.3-12}$$

$$\rho_{ij} = -\left(S_{ii}^* \times S_{ij} + S_{ji}^* \times S_{jj} \right), \text{ i and j=1 or 2} \tag{4.3-13}$$

In comparison with the reference antenna, there is minimal frequency shift in the CCL of the proposed MIMO CPDRA, showing little to no observable changes at the intercepting frequency point at 3.5 GHz. Nevertheless, the proposed CPDRA still exhibits a response lesser than 0.1 bits/Hz/sec over the operation band as illustrated in Figure 4.3-3.

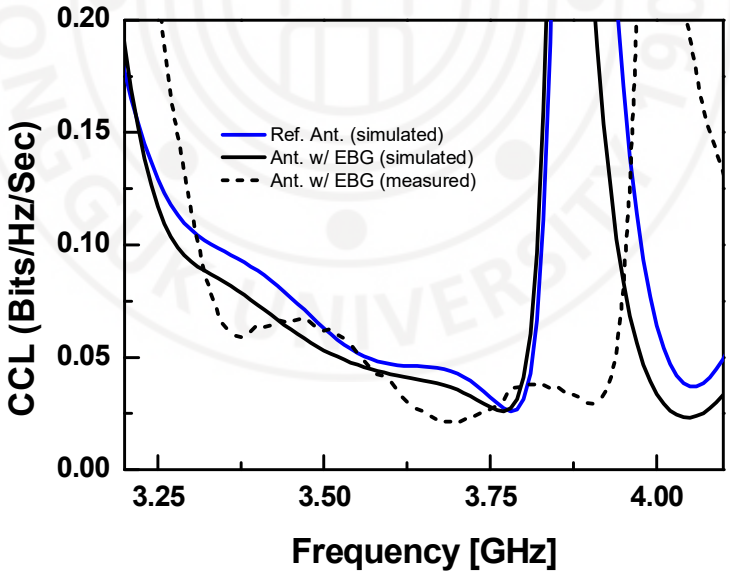

Figure 4.3-3 Channel capacity loss (CCL) comparison for antenna with and without EBG

4.4 Comparison with State-of-the-Art MIMO CPDRAs

Table 4.3-1 provides a comparison of the proposed MIMO CPDRA and existing related designs in the literature. As of date, there is very little research on CP MIMO DRAs due to its complexity in maintaining CP performance while possessing reasonably low mutual coupling. References [34] to [37] are designs with pattern diversity, polarization diversity and dual polarization with triple band features. The design in [38] has achieved a wide CP performance with high isolation. However, it was compromised with a significantly large antenna size.

The following table compares the measured results of the main parameter isolation and the diversity analysis parameters of ECC, DG and CCL as previously mentioned. Antenna size is included in the final column to demonstrate the compactness of proposed designs. Thus, the comparison has shown that the proposed MIMO CPDRA has a good isolation and diversity performance in a relatively compact size.

Table 4.4-1 Diversity comparison of proposed antenna with other reported CP MIMO DRAs

Ref.	Isolation (dB)	ECC	DG	CCL	Antenna Size (mm^2)
[34]	>18	<0.05	>9.96	NA	0.92 λ_0×0.92 λ_0
[35]	>25	<0.04	>9.16	NA	0.96 λ_0×0.77 λ_0
[36]	>20	<0.10	>8.50	NA	1.04 λ_0×1.62 λ_0
[37]	>18	<0.06	>9.90	<0.23	1.33 λ_0×0.95 λ_0
[38]	> 28	<0.04	>8.00	NA	4.33 λ_0×4.33 λ_0
This Work	**> 26**	**<0.03**	**>9.80**	**<0.10**	**1.09 λ_0× 0.56 λ_0**

Chapter 5 CONCLUSION

A wideband CPDRA is proposed in this thesis. To achieve a wideband AR performance, 45° partial truncation is applied at two diagonal edges of the DR merged with a cross-ring coupling slot at an optimum ratio. The adhesive effects occurred when attaching the DR to the PCB with coupling feeding structure was investigated and measurement results showed that 3-dB AR bandwidth is severely degraded. Miniature triangular stands were placed at the bottom part of the DR to attach it on the PCB, which prevented any adverse effects. The proposed antenna demonstrated measured impedance (S_{11}) and AR bandwidths of 25.9% and 18.7%, respectively, which accommodates the frequency band of 5G application systems (3.3–3.8 GHz) in the Republic of Korea. Furthermore, the MIMO array configuration with EBG structure engraved through ground plane was implemented and revealed promising isolation performance of –26 dB while maintaining its compact size. The antenna is further validated with the diversity analysis in section 4.3.

Up to 2 array elements for MIMO CP DRAs have been investigated in literature so far. For future improvements, the array number can be increased gradually to meet advanced high gain requirement wireless communication systems. However, such approach may generate complications such as maintaining wideband CP performance and will require more strategic solutions to facilitate the design.

REFERENCES

[1] R.D. Richtmyer, “Dielectric resonators,” *J. Appl. Phys.*, vol. 10, pp. 391 – 398, June 1939.

[2] A. Okaya, and L. Barash, "The Dielectric Microwave Resonator," *Proceedings of the IRE*, vol. 50, pp. 2081-2092, Oct. 1962.

[3] S. Long, M. McAllister, and L. Shen, “The resonant cylindrical dielectric cavity antenna,” *IEEE Trans. Antennas Propag*., vol. 31, no. 3, pp. 406-412, May 1983.

[4] G. P. Junker, D. Kajfez, A. A. Kishk and A. W. Glisson, "Effect of aperture filling on slot-coupled dielectric resonator antennas operating in HEM/sub 11/ mode," in *Electronics Letters*, vol. 31, no. 10, pp. 774-775, 11 May 1995.

[5] R. Q. Lee and R. N. Simons, "Bandwidth enhancement of dielectric resonator antennas, "*Proceedings of IEEE Antennas and Propagation Society International Symposium*, Ann Arbor, MI, USA, 1993, pp. 1500-1503 vol.3.

[6] Luk, K. M., Leung, K. W. and Chow, K. Y. (1997), Bandwidth and gain enhancement of a dielectric resonator antenna with the use of a stacking element. *Microw. Opt. Technol. Lett.*, 14: 215-217.

[7] K. W. Leung, K. Y. Chow, K. M. Luk and E. K. N. Yung, "Excitation of dielectric resonator antenna using a soldered-through probe," in *Electronics Letters*, vol. 33, no. 5, pp. 349-350, 27 Feb. 1997.

[8] R. K. Mongia, A. Ittipiboon, M. Cuhaci and D. Roscoe, "Radiation Q-factor of rectangular dielectric resonator antennas: theory and experiment," *Proceedings of IEEE Antennas and Propagation Society International Symposium and URSI National Radio Science Meeting*, Seattle, WA, USA, 1994, pp. 764-767 vol.2.

[9] A. Petosa, A. Ittipiboon, M. Cuhaci and R. Larose, "Bandwidth improvement for a microstrip-fed series array of dielectric resonator antennas," in *Electronics Letters*, vol. 32, no. 7, pp. 608-609, 28 March 1996.

[10] K. M. Luk and K. W. Leung, Eds., *Dielectric Resonator Antennas*. Baldock, UK: Research Studies, 2003.

[11] S. Gao, Q. Luo, and F. Zhu, *Circularly polarized antennas*, Wiley-IEEE Press, New York, November 2013.

[12] K. W. Leung, E. H. Lim, and X. S. Fang, “Dielectric resonator antennas: From the basic to the aesthetic,” *Proc. IEEE*, vol. 100, no. 7, pp. 2181-2193, Jul. 2012.

[13] G. Massie, M. Caillet, M. Clénet, and Y. M. M. Antar, “A new wideband circularly polarized hybrid dielectric resonator antenna,” *IEEE Antennas Wireless Propag. Lett*., vol. 9, pp. 347-350, Feb. 2010.

[14] Y. Pan, K. W. Leung, and E. H. Lim, “Compact wideband circularly polarized rectangular dielectric resonator antenna with dual underlaid hybrid couplers,” *Microw. Opt. Technol. Lett.*, vol. 52, no. 12, pp. 2789-2791, Dec. 2010.

[15] R. Chair, S. L. S. Yang, A. A. Kishk, K. F. Lee, and K. M. Luk, ″Aperture fed wideband circularly polarized rectangular stair shaped dielectric resonator antenna,” *IEEE Trans. Antennas Propag*., vol. 54, no. 4, pp. 1350-1352, Apr. 2006.

[16] M. I. Sulaiman and S. K. Khamas, "A Singly Fed Rectangular Dielectric Resonator Antenna with a Wideband Circular Polarization," in *IEEE Antennas and Wireless Propagation Letters*, vol. 9, pp. 615-618, 2010.

[17] K. Lu, K. W. Leung and Y. M. Pan, "Theory and Experiment of the Hollow Rectangular Dielectric Resonator Antenna," in *IEEE Antennas and Wireless Propagation Letters*, vol. 10, pp. 631-634, 2011.

[18] Y. M. Pan and K. W. Leung, "Wideband Omnidirectional Circularly Polarized Dielectric Resonator Antenna With Parasitic Strips," in *IEEE Transactions on Antennas and Propagation*, vol. 60, no. 6, pp. 2992-2997, June 2012.

[19] Y. M. Pan, K. W. Leung and K. Lu, "Omnidirectional Linearly and Circularly Polarized Rectangular Dielectric Resonator Antennas," in *IEEE Transactions on Antennas and Propagation*, vol. 60, no. 2, pp. 751-759, Feb. 2012.

[20] M. Khalily, M. R. Kamarudin, and M. H. Jamaluddin, “A novel square dielectric resonator antenna with two unequal inclined slits for wideband

circular polarization," *IEEE Antennas Wireless Propag. Lett.*, vol. 12, pp. 1256-1259, Sep. 2013.

[21] A. Buerkle, K. Sarabandi and H. Mosallaei, "Compact slot and dielectric resonator antenna with dual-resonance, broadband characteristics," in *IEEE Transactions on Antennas and Propagation*, vol. 53, no. 3, pp. 1020-1027, March 2005.

[22] X. Wang, L. Sun, X. Lu, S. Liang and W. Lu, "Single-Feed Dual-Band Circularly Polarized Dielectric Resonator Antenna for CNSS Applications," in *IEEE Transactions on Antennas and Propagation*, vol. 65, no. 8, pp. 4283-4287, Aug. 2017.

[23] J. Pan and M. Zou, "Wideband hybrid circularly polarised rectangular dielectric resonator antenna excited by modified cross-slot," *Electron. Lett.*, vol. 50, no. 16, pp. 1123-1125, Jul. 2014.

[24] X. Fang, K. W. Leung, and E. H. Lim, "Singly-fed dual-band circularly polarized dielectric resonator antenna," *IEEE Antennas Wireless Propag. Lett.*, vol. 13, pp. 995-998, May 2014.

[25] N. Yang, K. W. Leung, K. Lu and N. Wu, "Omnidirectional Circularly Polarized Dielectric Resonator Antenna with Logarithmic Spiral Slots in the Ground," *IEEE Transactions on Antennas and Propagation*, vol. 65, no. 2, pp. 839-844, Feb. 2017.

[26] R. Kumar and R. K. Chaudhary, "Circularly polarized rectangular DRA coupled through orthogonal slot excited with microstrip circular ring feeding structure for Wi-MAX applications," *Int. J. RF Microw. Comput. Aided Eng.*, vol. 28, pp. e21153, Jan. 2018.

[27] X. Chen, S. Zhang and Q. Li, "A Review of Mutual Coupling in MIMO Systems," in *IEEE Access*, vol. 6, pp. 24706-24719, 2018.

[28] M. S. Sharawi, A. B. Numan, and D. N. Aloi, "Isolation Improvement in a Dual-Band Dual-Element MIMO Antenna System Using Capacitively Loaded Loops," *Progress In Electromagnetics Research*, Vol. 134, 247-266, 2013.

[29] K. Trivedi, and D. Pujara, "Mutual coupling reduction in wideband tree shaped fractal dielectric resonator antenna array using defected ground

structure for MIMO applications," *Microw Opt Technol Lett*. vol. 59, no.11, pp. 2735–2742, Nov. 2017.

[30] K. Trivedi and D. Pujara, "Mutual Coupling Reduction in UWB Modified Maltese Shaped DRA Array for MIMO Applications," *2018 48th European Microwave Conference (EuMC)*," Madrid, 2018, pp. 1117-1120.

[31] M. J. Al-Hasan, T. A. Denidni, and A. R. Sebak, ''Millimeter wave compact EBG structure for mutual coupling reduction applications,'' *IEEE Trans. Antennas Propag*., vol. 63, no. 2, pp. 823–828, Feb. 2015.

[32] A. Dadgarpour, B. Zarghooni, B. S. Virdee, T. A. Denidni and A. A. Kishk, "Mutual Coupling Reduction in Dielectric Resonator Antennas Using Metasurface Shield for 60-GHz MIMO Systems," in *IEEE Antennas and Wireless Propagation Letters*, vol. 16, pp. 477-480, 2017.

[33] M. Farahani, J. Pourahmadazar, M. Akbari, M. Nedil, A. R. Sebak and T. A. Denidni, "Mutual Coupling Reduction in Millimeter-Wave MIMO Antenna Array Using a Metamaterial Polarization-Rotator Wall," in *IEEE Antennas and Wireless Propagation Letters*, vol. 16, pp. 2324-2327, 2017.

[34] N. K. Sahu, K. Das, and R. K. Gangwar, "Dielectric resonator-based wideband circularly polarized MIMO antenna with pattern diversity for WLAN applications," *Microw. Opt. Technol. Lett.*, vol. 60, no. 12, pp. 2855-2862, Dec. 2018.

[35] G. Das, A. Sharma, and R. K. Gangwar, "Dielectric resonator based circularly polarized MIMO antenna with polarization diversity," *Micorw. Opt. Lett.*, vol. 60, no. 3, pp. 685-693, Mar. 2018.

[36] A. Sharma, G. Das, and R. K. Gangwar, "Dual polarized triple band hybrid MIMO cylindrical dielectric resonator antenna for LTE2500/WLAN/WiMAX applications," *Int. J. RF Microw. Comput. Aided Eng.*, vol. 26, no. 9, pp. 763-772, Nov. 2016.

[37] N. K. Sahu, G. Das, and R. K. Gangwar, "Dual polarized triple-band dielectric resonator antenna based hybrid MIMO antenna for WiMAX/WLAN applications." *Microw. Opt. Technol. Lett.*, vol. 60, no. 4, pp. 1033-1041, Apr. 2018.

[38] J. Iqbal, U. Illahi, M. I. Sulaiman, M. M. Alam, M. M. Su'ud and M. N. Mohd Yasin, "Mutual Coupling Reduction Using Hybrid Technique in Wideband Circularly Polarized MIMO Antenna for WiMAX Applications," in *IEEE Access*, vol. 7, pp. 40951-40958, 2019.

[39] A.S..S., Neto, M.L., Dantas, J.S. Silva and H.C.C, Fernandes, "Antenna for Fifth Generation (5G) Using a EBG Structure," in *Springer International Publishing*, vol 354, pp. 33-38, 2015

[40] A. Annunziato, "5G Vision: NGMN - 5G Initiative," *2015 IEEE 81st Vehicular Technology Conference (VTC Spring)*, Glasgow, 2015, pp. 1-5.

[41] FierceWireless. *Q&A: Samsung's Cheun boasts 5G milestones in Korea*. Available: https://www.fiercewireless.com/wireless/q-a-samsung-s-cheun-boasts-5g-milestones-korea

[42] R. Kumar Mongia and A. Ittipiboon, "Theoretical and experimental investigations on rectangular dielectric resonator antennas," in *IEEE Transactions on Antennas and Propagation*, vol. 45, no. 9, pp. 1348-1356, Sept. 1997.

[43] Y. M. M. Antar and Z. Fan, "Theoretical investigation of aperture-coupled rectangular dielectric resonator antenna," in *IEEE Proceedings - Microwaves, Antennas and Propagation*, vol. 143, no. 2, pp. 113-118, April 1996.

[44] X. S. Fang and K. W. Leung, "Designs of single-, dual-, wide-band rectangular dielectric resonator antennas," *IEEE Trans. Antennas Propag.*, vol. 59, no. 6, pp. 2409-2414, Jun. 2011.

[45] A. Petosa, *Dielectric Resonator Antenna Handbook*. Norwood, MA, USA: Artech House, 2007.

[46] Chih-Yu Huang, Jian-Yi Wu and Kin-Lu Wong, "Cross-slot-coupled microstrip antenna and dielectric resonator antenna for circular polarization," in *IEEE Transactions on Antennas and Propagation*, vol. 47, no. 4, pp. 605-609, April 1999.

[47] Z. Zhang, X.-M. Wang, Y.-C. Jiao, and Z.-B Weng, "Broadband circularly polarized dielectric resonator antenna with annular slot excitation," *Prog. Electromagn. Res. C*, vol. 40, 105-117, Jan. 2013.

[48] A. M. Faiz, N. Gogosh, S. A. Khan, and M. F. Shafique, “Effects of an ordinary adhesive material on radiation characteristics of a dielectric resonator antenna.” *Microw. Opt. Technol. Lett.*, vol. 56, no. 6, pp. 1502-1506, Mar. 2014.

[49] C. Sarkar, D. Guha, and C. Kumar, “Glueless compound ground technique for dielectric resonator antenna and arrays,” *IEEE Antennas Wireless Propag. Lett.*, vol. 16, pp. 2440-2443, Jul. 2017.

[50] A. Rashidian, L. Shafai, and D. M. Klymyshyn, “Compact wideband multimode dielectric resonator antennas fed with parallel standing strips,” *IEEE Trans. Antennas Propag.*, vol. 60, no. 11, pp. 5021-5031, Nov. 2012.

[51] J. Y. Yin, X. Wan, J. Ren, and T. J. Cui, “A circular polarizer with beamforming feature based on frequency selective surfaces,” *Sci. Rep.*, vol. 7, pp. 41505, Jan. 2017.

[52] F. Yang and Y. Rahmat-Samii, *Electromagnetic Band Gap Structures in Antenna Engineering*, U.K: Cambridge Univ. Press, 2009.

[53] R. Coccioli, Fei-Ran Yang, Kuang-Ping Ma and T. Itoh, "Aperture-coupled patch antenna on UC-PBG substrate," in *IEEE Transactions on Microwave Theory and Techniques*, vol. 47, no. 11, pp. 2123-2130, Nov. 1999.

[54] E. Rajo-Iglesias, Ó. Quevedo-Teruel and L. Inclan-Sanchez, "Mutual Coupling Reduction in Patch Antenna Arrays by Using a Planar EBG Structure and a Multilayer Dielectric Substrate," in *IEEE Transactions on Antennas and Propagation*, vol. 56, no. 6, pp. 1648-1655, June 2008.

[55] S. D. Assimonis, T. V. Yioultsis and C. S. Antonopoulos, "Computational Investigation and Design of Planar EBG Structures for Coupling Reduction in Antenna Applications," in *IEEE Transactions on Magnetics*, vol. 48, no. 2, pp. 771-774, Feb. 2012.

[56] A. I. Najam, Y. Duroc and S. Tedjini, “Multiple-Input Multiple-Output Antennas for Ultra Wideband Communications,” in *Ultra Wideband – Current Status and Future Trends*, M. A. Matin, Ed., Rijeka, Crotia: Intech, 2012, pp. 210 – 236.

[57] S. Blanch, J. Romeu and I. Corbella, "Exact representation of antenna system diversity performance from input parameter description," in *Electronics Letters*, vol. 39, no. 9, pp. 705-707, 1 May 2003.

[58] K. Rosengren, P. S. Kildal, “Radiation efficiency, correlation, diversity gain and capacity of a six-monopole antenna array for a MIMO system. Theory, simulation, and measurement in reverberation chamber,” *IET Microw., Ant. and Propag.,* vol. 153, 2006, pp. 1-16, 2006.

[59] A. Iqbal, O. A. Saraereh, A. W. Ahmad and S. Bashir, "Mutual Coupling Reduction Using F-Shaped Stubs in UWB-MIMO Antenna," in *IEEE Access*, vol. 6, pp. 2755-2759, 2018.

[60] S. Ho-Chae, S. K. Oh, S. O. Park, “Analysis of mutual coupling, correlations, and TARC in WiBro MIMO array antenna,” *IEEE Antennas Wireless Propag. Lett.*, vol. 6, pp. 122-125, 2007.

[61] R. Kumar and R. K. Chaudhary, “A new modified CPW-fed wideband circularly polarized half-split cylindrical dielectric resonator antenna with different permittivity of two layers in radial direction,” in *Int J RF Microw Comput. Aided Eng*, vol. 27, no. 3, March 2017.

[62] M. I. Sulaiman and S. K. Khamas, “A singly fed wideband circularly polarized dielectric resonator antenna using concentric open half-loops,” *IEEE Antennas Wireless Propag. Lett.*, vol. 10, pp. 1305-1308, Nov. 2011.

[63] S. Trinh-Van, Y. Yang, K.-Y. Lee, and K.C. Hwang, “A wideband circularly polarized pixelated dielectric resonator antenna,” *Sensors*, vol. 16, no. 9, pp. 1349, Sep. 2016.